

University of Nevada, Reno

Crop Phenotyping of *Sorghum bicolor*'s Physiological Response to Salt-Affected Soils Using TLS and GPR Remote Sensing Technologies in Nevada Drylands

by

Erin L. Smith

Dr. Robert A Washington-Allen/Thesis Advisor

August, 2023

Copyright by Erin L. Smith 2023

All Rights Reserved



THE GRADUATE SCHOOL

We recommend that the thesis
prepared under our supervision by

Erin L. Smith

entitled

**Crop Phenotyping of Sorghum bicolor's physiological
response to Solonetz soils using TLS and GPR remote
sensing technologies in Nevada Drylands**

be accepted in partial fulfillment of the
requirements for the degree of

MASTER OF SCIENCE

Robert A. Washington-Allen
Advisor

Melinda K. Yerka
Committee Member

Paul S. Verburg
Graduate School Representative

Markus Kemmelmeier, Ph.D., Dean
Graduate School

August, 2023

Abstract

Saline and sodic soils are major abiotic stressors on the production of flood-irrigated crops in drylands. We conducted a crop phenotyping, remote sensing study on five genotypes of sorghum [*Sorghum bicolor* (L.) Moench], a drought and salt-tolerant crop, to assist in the molecular breeding of salt-tolerant cultivars. A control plot and a spatially heterogeneous saline-sodic plot (treatment plot) were established in collaboration with Dr. Yerka, Mr. Alfredo Delgado, Dr. Washington-Allen, the Nevada Agricultural Experiment Station (NAES) and the United States Department of Agriculture's Plant Materials Center (USDA-PMC) in Fallon, Nevada. This location is representative of the variable salinity/sodicity conditions typical of Northern Nevada soils and associated belowground biomass dynamics in drylands. We generated pre- and post-harvest soil attribute maps of the treatment plot using spatial interpolation, we expected individual genotypes to be affected differently by the gradient of various soil constituents. We hypothesized that above- and belowground three-dimensional structural phenology of the five genotypes would be differently affected across the salinity gradient in the treatment plot relative to the control plot. Additionally, we hypothesized that the GPR signal return would vary with the salinity gradient. Finally, we expected an increase in belowground biomass, relative to the control plot, in response to salt-stress as an adaptation to drought. The phenology of coarse-root depth and three-dimensional structure from pre-planting to harvest was non-invasively measured 15 times using a real-time kinematic (RTK) GPS-mounted IDS GeoRadar dual channel (400MHz and 900MHz) ground penetrating radar (GPR) system. Plant height and three-dimensional structural phenology of the five varieties were mapped using a FARO Focus3D X 330 terrestrial laser scanner (TLS). We found differences in above- and belowground three-dimensional structural phenology across the five genotypes in response to the salinity and sodicity gradient. Of the five genotypes in this study, only four

emerged in the treatment plot, where Richardson Seed's Ultra-Early Hybrid performed best under the gradient of salinity and sodicity with the highest rate of emergence (68%), the highest rate of panicle production (4.1 panicles per row), and the greatest panicle volume (67.2%) relative to the control plot. Furthermore, we found that the GPR return signal was not able to detect root mass in the highly saline-sodic soil, however, I was able to detect root mass phenology in the control plot. GPR return signal was not linear in response to the salinity gradient, however, a signal pattern emerged from the different salinity ranges suggesting a gradient response. This study shows the efficacy of the use of these technologies in crop phenotyping and precision agriculture. Future work may improve TLS derived data processing efficiency by developing methods for automating the detection of phenotypic traits (e.g., panicles, leaf area index, number of individual plants). These methods likely will include machine learning algorithms, allometric equations for biomass calculations, and use of drone-mounted LiDAR to reduce occlusion. The use of GPR in the salt-affected soils of this study was not able to definitively identify root mass, however, its use in soil composition for salts and other constituents is indeed promising. Further testing of GPR's non-detect threshold in salt-affected soils and its ability to quantify individual soil constituents has potential to be highly valuable to the field of soil science and precision agriculture. Furthermore, this study was able to detect a root mass response using GPR, future work may focus on differentiating genotypic variation in root phenology.

Acknowledgements

First, thank you to my major advisor Dr. Robert A. Washington-Allen for accepting me as a graduate student in the Environmental Tomography & Emerging Technologies Laboratory and for funding me as a graduate research assistant with the following funding sources: USDA-NIFA, NAES Multistate Project (Award #NEV00769) and US National Science Foundation, RAPID (Award #2141804). His mentorship and patience were unparalleled. Thank you to my committee member Dr. Melinda K. Yerka, who helped me to understand plant physiology and was foundational to the creation of this work. Thank you to Dr. Paul S. Verburg who was an insightful resource for all questions concerning saline and sodic soils and provided helpful advice regarding methods for soil data collection. Also, thank you to Alfredo Delgado for participating in the establishment of this study and providing GPR technical support. Thank you to the members of the Fallon, Nevada Plant Material Center for assistance with planting, irrigation and equipment. A big thank you to my comrades in the “Double Alien Lab” for their help with field work, equipment troubleshooting, methods for data processing, and emotional support that were crucial to my success as a graduate student. Thank you for the financial support from the UNR Graduate School’s Robert E. Dickenson Scholarship; and thanks to UNR for supplementary financial support during the COVID-19 pandemic. Thank you to my friends and family whose support and phone calls helped me get past the hurdles of graduate life and all the other chaos. Thank you to my dog Geronimo who became a therapy dog throughout this process. Finally, thank you to my loving partner Mike Elam who has supported me, encouraged me, challenged me, and made a lot of dinners making this experience possible.

Table of Contents

Abstract	i
Acknowledgements	iii
List of Tables	vi
List of Figures	vii
List of Equations	viii
Acronyms	ix
CHAPTER 1	1
1.1 Introduction	2
1.2 Global Significance of Sorghum	5
1.3 Salt-Affected Soils	6
1.3.1 Remediation Practices for Salt-Affected Soils	8
1.4 Emerging Technologies for High-Throughput Phenotyping	10
1.4.1 Terrestrial Laser Scanning Technology	10
1.4.2 TLS-Based Aboveground Crop Phenotyping	12
1.4.3 Ground Penetrating Radar Technology	13
1.4.4 GPR and Saline-Sodic Soil Conditions	14
1.4.5 GPR-Based Belowground Root Phenotyping	14
REFERENCES	17
CHAPTER 2 Tracking the above- and belowground phenology and physiological response of <i>Sorghum bicolor</i> to highly saline-sodic soils using lidar and radar technologies in Fallon, Nevada, United States	

2.1 Introduction	27
2.2 Materials and Methods	32
2.2.1 Study Area	33
2.2.2 Trait Response to Various Soil Constituents	34
2.2.3 Planting	38
2.2.4 TLS and GPR Field Sampling	40
2.2.5 TLS Data Processing and Analysis	43
2.2.6 GPR Data Processing and Analysis	46
2.3 Results	48
2.3.1 Aboveground Phenology and Response to Treatments	48
2.3.2 Height Response to Various Soil Constituents	49
2.3.3 Belowground Phenology and Response to Treatments	52
2.3.4 Biomass Response to Treatments	54
2.3.5 Manually Collected Biomass	56
2.4 Discussion	57
2.4.1 Aboveground Sorghum Response to Salinity Treatments	57
2.4.2 Belowground Root Monitoring and Response	59
2.4.3 Biomass Response to Salinity Treatments	60
2.5 Considerations for Further Study	61
2.5.1 Terrestrial Laser Scanning	61
2.5.2 Ground Penetrating Radar	63
2.6 Conclusions	64
REFERENCES	67

List of Tables

1.1	Salt-Affected Soils Criteria	8
2.1	Field Data Collection Schedule	41
2.2	TLS Equipment Specifications	42
2.3	GPR Equipment Specifications	43
2.4	Mean Height of Sorghum Genotypes by Treatment	49
2.5	Chi-Squared Test for Mean Height	49
2.6	GLM of Treatment Plot Height to Soil Constituents	51
2.7	Shapiro-Wilks Test of GLM Residuals	51
2.8	Regression of 400MHz Signal Return to Unplanted Rows	53
2.9	Regression of 900MHz Signal Return to Unplanted Rows	53
2.10	Survivability Rate in Treatment Plot	54
2.11	Chi-Squared Test for Survivability in Treatment Plot	54
2.12	Panicle Production Ration in Treatment Plot	55
2.13	Manual Biomass Collection Results	56
2.14	Ration of Mean Above- to Belowground Biomass Weights	57

List of Figures

2.1	Project Location Map	33
2.2	Control Plot Layout	35
2.3	Treatment Plot Layot	37
2.4	Control Plot Genotype Randomization	39
2.5	Treatment Plot Genotype Randomization	40
2.6	Clipped Point Clouds with Panicle Segmentation	44
2.7	TLS Data Processing Work Flow	45
2.8	GPR Data Processing Work Flow	47
2.9	TLS-Derived Height Phenology	48
2.10	Correlation Matrix of Treatment Plot Soil Constituents	50
2.11	Root Phenology of Control Plot at 400MHz and 900MHz	52
2.12	Point Cloud Comparison of Panicle Mass	56

List of Equations**Equation 1:**

$$ESP = \frac{\text{Exchangeable Sodium}}{\text{Cation Exchange Capacity}} * 100$$

Equation 2:

$$SAR = \frac{Na^+}{(Ca^{2+} + Mg^{2+})^{0.5}}$$

Equation 3:

$$d = [c * t] / 2$$

Equation 4:

$$\mathcal{E}_r = (c/V)^2$$

Acronyms

UNR - University of Nevada, Reno

USDA-PMC - United States Department of Agriculture Plant Materials Center

LiDAR - Light detection-and-ranging

RADAR - Radio detection-and-ranging

TLS - Terrestrial laser scanner

GPR - Ground penetrating radar

RTK-GPS - Real-time kinematic global positioning system

ESP - Exchangeable sodium percentage

SAR - Sodium adsorption ratio

ECe - Electrical conductivity

FAO - Food and Agriculture Organization of the United Nations

NRCS - USDA Natural Resources Conservation Service

TOF - Time-of-flight

EMR - Electromagnetic radiation

ϵ_r - Relative permittivity

UAV - Unmanned aerial vehicles

TDR - Time domain reflectometer

CHAPTER 1

Review

Erin L. Smith¹

- 1 Department of Agriculture, Veterinary & Rangeland Science, University of Nevada, Reno, Reno, NV, erinlsmith@nevada.unr.edu

Abstract: Drylands cover approximately 41.3 percent of the Earth's land surface and are home to 38 percent of the global population. These areas are often underestimated or seen as less productive, however, drylands contribute 44 percent to global crop production and are valued at approximately \$18 Trillion in ecosystem services. Crop production in drylands is increasingly limited by increasing temperatures, aridity, and soil salinization. Saline and sodic soils are major abiotic stressors on the production of irrigated crops in drylands. An estimated 230Mha of irrigated land globally is impacted by salinization. Additionally, belowground biomass estimates in drylands are uncertain, particularly because belowground estimates are at times uncoupled from aboveground estimates. We conducted a crop phenotyping, remote sensing study on five genotypes of sorghum [*Sorghum bicolor* (L.) Moench], a drought and salt-tolerant crop, to assist in the molecular breeding of salt-tolerant cultivars adapted to the climatic and edaphic conditions common to northern Nevada. Sorghum is widely planted across drylands due to its relatively higher tolerance to drought, heat, and salt stress. A non-saline/non-sodic control plot and a spatially heterogeneous saline-sodic plot (treatment plot) were established in Fallon, Nevada. This location is representative of the variable salinity conditions typical of Northern Nevada soils as well as a model site for belowground biomass dynamics in drylands. We generated pre- and post-harvest soil attribute maps of the control plot and treatment plot using spatial interpolation.

We hypothesized that above- and belowground three-dimensional structural phenology of the five genotypes would be differently affected across the flood irrigated salinity gradient.

Phenology of coarse-root depth and three-dimensional structure from pre-planting to harvest was non-invasively measured 15 times using a real-time kinematic (RTK) GPS-mounted IDS GeoRadar dual channel (400MHz and 900MHz) ground penetrating radar (GPR) system. Plant height and three-dimensional structural phenology of the five varieties were mapped using a FARO Focus3D X 330 terrestrial laser scanner (TLS).

1.1. Introduction

The ancient grain sorghum [*Sorghum bicolor* (L.) Moench], also known commonly as sweet sorghum, millet, milo, and durra, is a staple cereal crop for many global populations, particularly those found in arid regions. Sorghum is often widely planted in dry climates due to its relatively higher tolerance to abiotic and edaphic stressors such as drought, high temperatures, and salt-affected soils, which negatively impact crop production and contribute to issues of global food insecurity [1]. For its relative success under these stressful conditions, sorghum is the fifth most grown cereal crop worldwide following maize, rice, wheat, and barley [2].

Drylands are water-limited regions with high rates of evapotranspiration and are defined by an aridity index between 0.03-0.65, which is the ratio of mean annual precipitation to mean annual evaporation [3,4]. These regions are often viewed as less productive, however, they contribute 44 percent of global crop production and have been valued at \$18 Trillion in ecosystem services [5]. Drylands make up more than 41.3 percent of the Earth's land surface and are home to 38 percent of the global population, approximately 2.1 billion people, the majority of whom are

critically poor [6,7]. Drylands are experiencing expansion resulting from increasing aridity and higher temperatures caused by climate change [8,9].

Small farmers and rural communities are at a particular disadvantage, as they are often without the resources to mitigate soil salinization or do not have access to increased irrigation water needed to cope with climate change [4,8-10]. Therefore, it is vitally important to develop sorghum varieties specifically adapted to these stressors and improve methods for efficient data collection through emerging technologies.

The *Sorghum* genus is a member of the Poaceae family of grasses, of which there are 24 recognized species. These various species of sorghum have been cultivated for a variety of uses such as biofuel, livestock forage, and alcohol production [2]. Beyond the species level, tolerance to various stressors can be further subdivided by individual genotype which can impact crop yield and other measures of resiliency, and can be significant at different stages of crop development.

The cereal grain species was cultivated from wild *Sorghum bicolor* and has been developed into a wide variety of cultivars through selective breeding. Cultivars of sorghum can be developed regionally, by selecting characteristics suited to specific environmental conditions. Cultivar development is typically a time-consuming process [11,12], requiring many generations of growth, close monitoring of phenology, and reoccurring measurements of above- and belowground biometrics.

Crop breeders use above- and belowground phenotypic traits (e.g., leaf area index (LAI), average height, biomass, panicle density, root depth, root volume, root mass) to compare genotype response to specific growing conditions. To measure the response of these phenotypic

indicators of resiliency to abiotic stressors, data are usually collected by means of destructive sampling, which is particularly true for collection of belowground data.

In crop breeding programs, destructive sampling is often done throughout the growing season at the various stages of development. The challenge of destructive sampling is selecting representative specimens and collecting a large enough sample size to be representative while also leaving enough material for iterative sampling. Additionally, this process can be slow, subjective, labor intensive, and sampled locations cannot be resampled, and these issues have the potential to introduce bias and misrepresentation into data.

This study compares the above- and the belowground response of five genotypes of early-emergent *Sorghum bicolor* to heterogeneous, highly-saline, and sodic soil conditions. This research assists an ongoing molecular breeding program for *Sorghum bicolor* at the University of Nevada, Reno (UNR), in collaboration with the United States Department of Agriculture Plant Materials Center (USDA-PMC) located in Fallon, Nevada, United States. The goal of this specific project is to develop sorghum cultivars best suited to the climatic and edaphic conditions found in Northern Nevada; however similar conditions occur throughout dryland ecosystems globally [7]. The broader goals are to (1) expand the frequency and scope of crop-response data to drought and saline-sodic soil conditions; and (2) develop methods for high-throughput and fine-grain data collection using emerging, non-invasive, remote sensing technologies.

Light detection-and-ranging (LiDAR) and radio detection-and-ranging (RADAR) were the two types of remote sensing technologies utilized in this study to non-invasively quantify phenotypic traits of sorghum throughout the growing season. Aboveground LiDAR data was collected using a terrestrial laser scanner (TLS) and belowground RADAR data was collected using ground penetrating radar (GPR). A benefit of using these technologies simultaneously

along with a real-time kinematic global positioning system (RTK-GPS), is that the above- and belowground data can be precisely paired, a result which is unprecedented in sorghum cultivation [13].

Creating a means of investigating crop traits in response to abiotic and edaphic stressors through remote sensing technologies is a step toward addressing the reliability of future food supplies and global food security. Therefore, it is crucial for plant phenotypic traits to be linked to physiological responses and genotypes that will aid in promoting resource efficiency and crop yields towards the development of a sustainable intensive agricultural system [14,15].

1.2. Global Significance of Sorghum

Sorghum bicolor is a flowering grass in the family *Poaceae* that is usually cultivated as an annual [16]. This cereal grain likely originated in Northeastern Africa near what is now Sudan and Ethiopia, most likely domesticated from a wild species sometime between 8,000 – 4,000 B.C.E. [17]. Since then, sorghum cultivation has spread regionally by various means, eventually being grown in over one hundred countries [18].

Presently, the United States produces the largest amount of grain sorghum annually. Its primary use is for the production of ethanol for biofuel and as livestock fodder [19]. Although the United States is the largest global producer, other dryland countries in Sub-Saharan Africa, Asia, South America, and the Caribbean dedicate a larger percentage of their arable land to sorghum cultivation, which is mainly used for human consumption [20]. Global production of grain sorghum is divided into two general groupings: countries that produce grain sorghum as a surplus for industrial purposes (e.g., the United States), and those that produce grain sorghum for human consumption or local trade (e.g., Sub-Saharan countries). Promoting international trade

and increasing crop productivity while also preserving the various uses of the plant will be important to maintain or grow the global significance of grain sorghum [20].

Within drier regions of the world, sorghum is grown primarily because of its morphological traits that confer drought tolerance. Sorghum has unique root traits that help establishment and resiliency during drought. These traits include the formation of a root system prior to rapid aboveground growth, an extensive secondary root system, and silica deposits in the endodermis of roots that prevents structural collapse under drought stress. Additionally, sorghum leaves have a waxy coating that can curl inward, reducing evapotranspiration during drought conditions but can resume growth when conditions improve [16].

1.3. Salt-Affected Soils

Salt stress can have a significant impact on plant growth. For example, it can inhibit net photosynthesis, metabolism, and protein synthesis. Only a limited number of plants can thrive, or even survive, in saline or sodic soils, also known as salt-affected soils. However, when salt-tolerant sorghum detects salt stress, cascades of endogenous hormones are initiated provoking numerous salt-stress responses [21]. These hormones can restrict the transport of sodium from the roots to the aboveground plant matter and allow maintenance of photosynthetic efficiency and accumulation of sucrose. Sorghum's tolerance to salt, multiple uses, and low input requirements are characteristics that make it an attractive alternative to other cereal grain crops that have much higher resource demands (e.g., rice, corn).

Salt-affected soils, which include saline soils, sodic soils, and saline-sodic soils, are among the most significant abiotic factors negatively impacting agricultural production and food security in arid and semi-arid regions [21]. Sources of salt can be naturally occurring through

saline groundwater, soluble complexes in rain water, eolian deposition, and weathering of saline parent material. They can also be anthropogenically created through the mismanagement of irrigation production systems [22].

In regions with greater precipitation, salts are often leached out of the soil profile, however, in arid climates where there are greater evaporative losses, salts will either leach very slowly or accumulate within the soil profile [23]. The impact of salinization, or the accumulation of water-soluble salts in soil, is projected to increase with climate change, co-occurring with more extreme variation in weather patterns [1,24]. Therefore, there is an impetus to manage salt-affected soils by selecting for drought-tolerant crops, which is an objective of this thesis.

Soluble salts include sodium, calcium, magnesium, chlorine, sulphate, and bicarbonate (i.e., Na^+ , Ca^{2+} , Mg^{2+} , Cl^- , SO_4^{2-} , and HCO_3^-), which can impact microbial activity, chemical properties, and physical structure, inhibiting seed germination, plant growth, and yield [25]. Saline, sodic, and saline-sodic soils are most commonly differentiated using the following metrics: pH of saturated soil paste, exchangeable sodium percentage (ESP), sodium adsorption ratio (SAR), and electrical conductivity (EC_e) [26-28]. Exchangeable sodium percentage is the fraction of adsorbed sodium on the soil exchange sites, where ESP is expressed as a percentage, (Equation 1); an ESP value above 15 percent is indicative of sodic soil. The sodium adsorption ratio quantifies the relationship between sodium and divalent cations (i.e., calcium and magnesium), in a water extract (Equation 2); a SAR value above 13 is another indicator of sodicity.

$$ESP = \frac{\text{Exchangeable Sodium}}{\text{Cation Exchange Capacity}} * 100 \quad (1)$$

$$SAR = \frac{\text{Na}^+}{(\text{Ca}^{2+} + \text{Mg}^{2+})^{0.5}} \quad (2)$$

Table 1.1. Differentiation of the types of salt-affected soils by chemical composition.

Salt-affected Soil Type	Sodium Adsorption Ratio (SAR)	Exchangeable Sodium Percentage (ESP)	Electrical Conductivity (dS m⁻¹)	Soil pH
Saline	< 13	≤ 15%	> 4	< 8.5
Sodic	≥ 13	≥ 15%	< 4	> 8.5
Saline-Sodic	≥ 13	≥ 15%	> 4	< 8.5

Soils are considered saline if they have EC_e values above 4dS m^{-1} , whereas sodic soils tend to have an EC_e below 4dS m^{-1} . Plant water uptake is inhibited by salt and solutes in the soil solution that lowers the water potential making it more difficult for plant roots to retrieve water from the soil. Often plants will also uptake some sodium along with water, and excessive ion uptake over time causes toxicity in the plant tissue [29].

Sodic soils or Solonetz soils (European & FAO classification system) typically have pH values at or above 8.5 and contain high relative proportions of sodium, which reduces nutrient availability to plants [30]. With sodium saturation greater than 15 percent and in the presence of fresh water, the high proportions of sodium and potassium cations and low proportion of divalent salts can cause clay particles to disperse and soil aggregates to collapse. As a result, wet soils have a jelly-like consistency, and when dry, may exhibit surface cracking [31]. A lack of soil aggregates affects drainage, induces hard setting, can cause soil surface sealing, and restricts water and oxygen movement, which can suffocate plant roots [32].

1.3.1. Remediation Practices for Salt-Affected Soils

Saline soils can be reclaimed by removing salts through leaching. There are three general management strategies for removing salts: 1) Leaching salts from the root zone by irrigating beyond what is needed by a plant; 2) Installation of belowground drains to move leachate out of

the root zone in a controlled manner; and 3) Leaching salts to another area in an irrigated field that does not impact plant growth [33].

Leaching salts, however, can induce other issues for crop production, such as the leaching of desired nutrients and pesticides, which could also risk contaminating surface or groundwater resources. Water quality is an important consideration when remediating for salinity; poor water quality can exacerbate salt accumulation in soils, particularly in arid climates where evaporation exceeds precipitation [34].

Sodic soils often have poor physical structure and drainage resulting from the deflocculation of clay particles, and therefore, often need amendments to restore aggregation. The objective of using amendments is to replace sodium with calcium and leach out the excess sodium. Typically gypsum (CaSO_4) is used as a source of Ca because it is easily soluble at high pH. If limestone or, calcium carbonate, is present in the soil, the addition of sulfur can lower the pH making the calcium from the lime available. Two basic management strategies are used to remediate sodic soils for crop production: 1) Change crop to a more sodium tolerant species, variety or genotype; and 2) Change the soil conditions with addition of amendments followed by leaching with increased irrigation to remove excess Na [33].

For many rural farmers remediating salt-affected soils with irrigation or amendments is often unfeasible, especially for those living in developing nations and relying on rain-fed agriculture. In the global drylands many farmers are without resources to accommodate the scale or significant time requirements for soil remediation [35,36]. An often more affordable and available alternative is changing crops to a variety or genotype that is more tolerant of salt, which, through careful management, can become vegetative bioremediation, a practice used in conservation agriculture [37,38]. Molecular breeding programs are important for developing cultivars capable

of growing under a variety of these edaphic conditions and has the potential to assist many disadvantaged people living in drylands.

1.4. Emerging Technologies for High-Throughput Phenotyping

In the coming decades, population growth and loss of arable land to climate change, pollution, and soil degradation are projected to exponentially increase global issues of food insecurity if not addressed [39]. Crop breeding programs that cultivate genotypes capable of producing higher yields under abiotic and edaphic stress are crucial for addressing these issues. High-throughput crop phenotyping is a process or method used by molecular breeding programs to rapidly select visible crop traits and train predictive genomic selection models [40]. However, efficient and affordable collection of fine-grained and high-quality data over geographically large agricultural fields remains challenging [41].

Emerging technologies such as the terrestrial laser scanning and ground penetrating radar can be used effectively for high-throughput data collection by crop breeders, as they offer high accuracy and precision [42-44]. Furthermore, these technologies are a quantitative and non-destructive approach to monitoring crop health and physiology through remote sensing [45].

1.4.1. Terrestrial Laser Scanning Technology

Terrestrial laser scanning, also known as ground-based LiDAR (light detection-and-ranging), is a type of active remote sensing that emits energy in the form of electromagnetic radiation (EMR) from the sensor to detect objects and materials in the surrounding environment [46]. There are two distinct types of TLS ranging systems: pulse-based or time-of-flight (TOF) and phase-shift [47].

Time-of-flight TLS is the most common type and consists of a laser transmitter that emits pulses of EMR in the visible or near infrared wavelength, a receiver channel, amplifiers, an automatic gain control, and timing discriminators. The emitted EMR pulse triggers a time interval measurement unit that records the time it takes for that pulse of EMR to travel to a target, reflect off the surface of that target, and be intercepted by the sensor. A single pulse is used for the unequivocal determination of range which is half of the round-trip distance and time traveled by the emitted photons. Equation 3 shows the basic range calculation for TOF sensors.

$$d = [c * t] / 2 \quad (3)$$

Where, c = speed of light, and t = time.

Phase-shift ranging uses interferometry where a specific wavelength of EMR is continuously emitted, but power is modulated at a constant frequency (phase), and the fraction of the whole wavelength returned is recorded. The scanner uses phase-shift algorithms to determine distance to an object, these are based on the unique properties of each individual phase, which calculate distance as a fraction of the modulated signal's wavelength.

Between pulse-based TLS and phase-based TLS, one main tradeoff is between the speed of acquisition and dynamic range. Time-of-flight systems often have longer scanning times since they initiate the EMR pulse only after the previous one is received. However, TOF systems typically offer greater scanning distance ranges than phase-shift systems. Phase-shift systems can be very precise, with ranging errors in the order of a few millimeters, but have much higher energy requirements. Thus, phase-based ranging is more often used for short-range scanning.

Both types of TLS have the capacity to collect three-dimensional structural data of targeted objects, a feature unique to this type of remote sensing [48]. Multiple scans of the same object or target, collected at different positions around the target, are registered together to create three-dimensional point clouds; this is a principal of structure from motion [41]. The high accuracy of TLS data allows measurements to be taken from the direct manipulation of three-dimensional point clouds and enables users to detect changes in spatial data sets over time [49].

1.4.2. TLS-Based Aboveground Crop Phenotyping

Most environmental applications of LiDAR to date have been in forestry, where it has been used to derive forest traits such as leaf area, tree height, diameter-at-breast-height, tree density, crown area, and biomass estimates of individual trees [47,48,50]. However, the application of TLS in agriculture studies is a relatively recent development. Now, TLS technology is being used to quantify agricultural parameters, such as plant height, three-dimensional structure, aboveground biomass, panicle density, and for predicting yield [50-53]. Depending on the wavelength of the EMR emitted by the TLS, other physiological characteristics and health metrics can be generated, such as plant water stress, leaf nitrogen status, and plant pigments such as chlorophyll *a* and *b*, and xanthophylls [54,55].

Most recently, TLS in conjunction with machine learning algorithms has been used to identify individual plants. TLS and adaptive learning technologies have been used to estimate the number of wheat tillers and has shown promising results at capturing phenology, though, results generally under estimated number of tillers due to occlusion issues [56]. However, manually counting tillers is incredibly labor intensive, often infeasible, and results are arguably subjective;

having a technology to automate this process can save an innumerable amount of time and resources, and has the potential to reduce human error.

Machine learning processes are also being used to identify individual panicles for improved yield estimates and for determining leaf base and inclination angles, leaf area, and stem diameter [57,58]. Using TLS technology, cultivars developed in crop breeding programs can be studied with enough spatial and temporal resolution to isolate specific physiological and agronomic traits of significance, for example, those adapted to abiotic stressors.

1.4.3. Ground Penetrating Radar Technology

Ground penetrating radar (GPR) uses RADAR technology and has applications in a wide array of scientific fields such as geology, soil science, archaeology, mining, biogeochemistry, and civil engineering. Pulses of EMR in the microwave range are emitted from the GPR transmitter to the subsurface, where the signal is either absorbed, scattered, or reflected off buried objects or substrates, and then detected by a receiver. The reflected energy returns are transformed into amplitude and a two-way travel time, from which substrate composition and depth can be determined. In general, lower frequencies are able to penetrate deeper belowground but have lower resolution than higher frequencies, which do not penetrate as deep but have higher resolution.

Electromagnetic properties such as EC_e , magnetic permeability, dielectric permittivity, or relative permittivity (ϵ_r), are important when trying to identify belowground objects [59]. Essentially, GPR is capable of detecting an object when there is a difference between the electromagnetic properties of the object and the soil. The relative permittivity of the soil is of great importance when determining effectiveness of the GPR signal for “seeing” belowground

(see Equation 4). Relative permittivity is the resistance of a material to an electrical field, where ϵ_r impacts the propagation of the electromagnetic signal from the GPR.

$$\epsilon_r = (c/V)^2 \quad (4)$$

Where c = speed of light, V = velocity of a given wavelength, and ϵ_r = relative permittivity

1.4.4. GPR and Saline-Sodic Soil Conditions

The use of GPR is limited in soils with higher EC_e and higher ϵ_r , these include soils with relatively higher clay contents and high volumetric water content. Such soils restrict the depth of signal penetration, return response, and signal resolution, and may cause signal scattering or attenuation. However, results can vary based on the frequency used [60], consequently, the use of GPR in salt-affected soil is limited [61,62]. Only a few studies have used GPR as a means to detect soil properties such as volumetric water content [59] and soil salinity, and none of these studies had the added objective of subsurface object detection [63,64]. We hypothesize that the GPR return signal for the 400MHz and 900MHz frequencies will vary linearly with the gradient of salinity in the treatment plot.

1.4.5. GPR-Based Belowground Root Phenotyping

Understanding crop root dynamics is necessary for optimizing agricultural production because crop roots anchor the plant and absorb the water and nutrients necessary for plant growth and grain production. Crop breeders want to understand the ability of a genotype's roots to adapt to selective pressures in order to develop cultivars with traits for specific growing environments [65]. In crop breeding programs, both above- and belowground phenotyping is used to train prediction models, identify genetic markers for later selection, and to study gene-

environment interactions. Crop phenotyping requires direct measurements of phenotypic traits of interest, however, measurements of root traits is limited by the current means of directly study roots that are often destructive or limited to greenhouse environments [66].

In-situ observation and monitoring of root growth is needed in crop breeding and can improve resource management and our knowledge of terrestrial biogeochemical cycling. However, this often requires removing roots from the ground and the destruction of the plant. Improved methods for root phenotyping involve a non-destructive iterative approach to allow crop breeders to track the belowground phenology of individual plants through time; this is otherwise not possible with destructive sampling. Non-destructive detection of *Sorghum bicolor* root phenology with GPR has not yet been attempted; other non-destructive technologies for root monitoring, such as a mini-rhizotron and X-ray, have been used. However, these methods provide only point-based data collection method [43]. This poses a challenge in interpolating point data to a plot-wide or field scale, given the spatial and temporal variation of soil conditions even in an agricultural field.

Currently, there is a lack of access to root phenotyping techniques that can quantify traits related to growth and yield. Most phenotyping is done through visual assessment by experts, which is time consuming and destructive, thereby limiting data collection potential for molecular breeding programs [67]. However, roots usually have a higher water content than the surrounding bulk soil, allowing GPR to detect a wide variety of physical root attributes, such as root depth, root mass, and root architecture [66].

Ground penetrating radar is a way to capture real-time, continuous data on root phenology in field conditions and can support molecular breeding programs aimed at developing cultivars adapted to specific environmental stressors. The potential for high-quality,

high-accuracy, high-throughput data collection with emerging technologies can be applied to crop breeding programs and precision agriculture, which is an important step toward improving yield and resiliency under abiotic and edaphic stress while also using fewer resources.

Consequently, the goals of this study were to develop salt tolerant cultivars of *Sorghum bicolor* for northern Nevada producers. This study was a genome-wide association study, of five of the approximately 400 sorghum genotypes in the Sorghum Association Panel, to identify genetic tolerances to salt stress. In this study I use TLS and GPR technologies to track the above- and belowground phenology of five genotypes of sorghum in a gradient of highly saline-sodic soil in a treatment plot, and in a control plot. I asked how a salinity gradient affects above- and belowground phenology of individual genotypes and which genotypes are more tolerant to this stressor. Additionally, I ask whether GPR can detect root mass in highly saline-sodic soil and if an observable difference in root response can be detected between salinity treatments and the control plot.

In this study I expected a difference in above- and belowground phenology of the five genotypes between the both the treatment and control plots. I expected individual genotypes to be affected differently by the gradient of soil characteristics in addition to salinity. I expected the GPR return signal to vary with the salinity gradient in the treatment plot. Finally, I expected an increase in belowground biomass in response to salt-stress, relative to the control plot.

REFERENCES

1. Cao, Li, Y., Liu, B., Kong, F., & Tran, L.-S. P. (2018). Adaptive Mechanisms of Soybean Grown on Salt-Affected Soils: Salt Adaptation in Soybean. *Land Degradation & Development*, 29(4), 1054–1064. <https://doi.org/10.1002/ldr.2754>
2. United Sorghum Checkoff Program: All About Sorghum, 2016. Available Online: <https://www.sorghumcheckoff.com/all-about-sorghum> (accessed on 21 May 2021).
3. Zomer, Trabucco, A., Bossio, D. A., & Verchot, L. V. (2008). Climate change mitigation: A spatial analysis of global land suitability for clean development mechanism afforestation and reforestation. *Agriculture, Ecosystems & Environment*, 126(1), 67–80. <https://doi.org/10.1016/j.agee.2008.01.014>
4. Berdugo, Delgado-Baquerizo, M., Soliveres, S., Hernández-Clemente, R., Zhao, Y., Gaitán, J. J., Gross, N., Saiz, H., Maire, V., Lehmann, A., Rillig, M. C., Solé, R. V., & Maestre, F. T. (2020). Global ecosystem thresholds driven by aridity. *Science (American Association for the Advancement of Science)*, 367(6479), 787–790. <https://doi.org/10.1126/science.aay5958>
5. Costanza, de Groot, R., Sutton, P., van der Ploeg, S., Anderson, S. J., Kubiszewski, I., Farber, S., & Turner, R. K. (2014). Changes in the global value of ecosystem services. *Global Environmental Change*, 26, 152–158. <https://doi.org/10.1016/j.gloenvcha.2014.04.002>
6. Corvalán, Hales, S., McMichael, A. J., Corvalán, C., McMichael, A. J., Corvalán, C. (Carlos), & McMichael, A. J. (Anthony J. . (2005). *Ecosystems and human well-being : health synthesis*. World Health Organization.
7. United Nations: Deserts, desertification, drylands, biodiversity, climate change, the environment. Available Online at: https://www.un.org/en/events/desertification_decade/whynow.shtml (accessed on 11 August 2021).
8. Huang, Yu, H., Guan, X., Wang, G., & Guo, R. (2016). Accelerated dryland expansion under climate change. *Nature Climate Change*, 6(2), 166–171. <https://doi.org/10.1038/nclimate2837>

9. Maestre, Eldridge, D. J., Soliveres, S., Kéfi, S., Delgado-Baquerizo, M., Bowker, M. A., García-Palacios, P., Gaitán, J., Gallardo, A., Lázaro, R., & Berdugo, M. (2016). Structure and Functioning of Dryland Ecosystems in a Changing World. *Annual Review of Ecology, Evolution, and Systematics*, 47(1), 215–237. <https://doi.org/10.1146/annurev-ecolsys-121415-032311>
10. Galieni, A., D'Ascenzo, N., Stagnari, F., Pagnani, G., Xie, Q., & Pisante, M. (2020/2021;). Past and future of plant stress detection: An overview from remote sensing to positron emission tomography. *Frontiers in Plant Science*, 11, 609155-609155.
11. Friedli, M., Kirchgessner, N., Grieder, C., Liebisch, F., Mannale, M., & Walter, A. (2016). Terrestrial 3D laser scanning to track the increase in canopy height of both monocot and dicot crop species under field conditions. *Plant Methods*, 12(1), 9-9.
12. Fang, Y., Qiu, X., Guo, T., Wang, Y., Cheng, T., Zhu, Y., Chen, Q., Cao, W., Yao, X., Niu, Q., Hu, Y., & Gui, L. (2020). An automatic method for counting wheat tiller number in the field with terrestrial LiDAR. *Plant Methods*, 16(1), 1-132.
13. Kuijken, van Eeuwijk, F. A., Marcelis, L. F. M., & Bouwmeester, H. J. (2015). Root phenotyping: from component trait in the lab to breeding. *Journal of Experimental Botany*, 66(18), 5389–5401. <https://doi.org/10.1093/jxb/erv239>
14. Rockstrom et al. 2017. Sustainable intensification of agriculture for human prosperity and global sustainability. *Ambio* 46:4 – 17.
15. Pretty, Jules. 2018. Intensification for redesigned and sustainable agricultural systems. *Science* 362, 908 and *Science* 362 eaav0294
16. Office of the Gene Technology Regulator. (2017). *The biology of Sorghum bicolor (L.) Moench Subsp. bicolor (sorghum)*. The OGTR.
17. McGinnis, M. J., & Painter, J. E. (2020). Sorghum: History, Use, and Health Benefits. *Nutrition Today (Annapolis)*, 55(1), 38–44. <https://doi.org/10.1097/NT.0000000000000391>

18. Visarada, K. B. R. S., & Aruna, C. (2021). Breeding Sorghum for Specific End Uses. In *Sorghum in the 21st Century: Food – Fodder – Feed – Fuel for a Rapidly Changing World* (pp. 453–482). Springer Singapore. https://doi.org/10.1007/978-981-15-8249-3_19
19. Paterson, Bowers, J. E., Bruggmann, R., Dubchak, I., Grimwood, J., Gundlach, H., Haberer, G., Hellsten, U., Mitros, T., Poliakov, A., Schmutz, J., Spannagl, M., Tang, H., Wang, X., Wicker, T., & Ware, D. (2009). Sorghum bicolor genome and the diversification of grasses. *Nature*, 457(7229), 551–556. <https://doi.org/10.1038/nature07723>
20. Tonapi, V. A. (2020). *Sorghum in the 21st century : food, fodder, feed, fuel for a rapidly changing world* (1st ed. 2020.). Springer. <https://doi.org/10.1007/978-981-15-8249-3>
21. Yang, Z., Li, J.-L., Liu, L.-N., Xie, Q., & Sui, N. (2019). Photosynthetic Regulation Under Salt Stress and Salt-Tolerance Mechanism of Sweet Sorghum. *Frontiers in Plant Science*, 10, 1722–1722. <https://doi.org/10.3389/fpls.2019.01722>
22. Schaetzl, R. J. and Thompson, M. L. (2016). *Soils: Genesis and geomorphology* (Second edition). Cambridge University Press.
23. Cuevas, Daliakopoulos, I. N., Fernando del Moral, Hueso, J. J., & Tsanis, I. K. (2019). A Review of Soil-Improving Cropping Systems for Soil Salinization. *Agronomy (Basel)*, 9(6), 295–. <https://doi.org/10.3390/agronomy9060295>
24. Qadir, M., & Oster, J. D. (2004). Crop and irrigation management strategies for saline-sodic soils and waters aimed at environmentally sustainable agriculture. *Elsevier B.V.*
25. Amini, Ghadiri, H., Chen, C., & Marschner, P. (2016). Salt-affected soils, reclamation, carbon dynamics, and biochar: a review. *Journal of Soils and Sediments*, 16(3), 939–953. <https://doi.org/10.1007/s11368-015-1293-1>
26. FAO Land and Plant Nutrition Management Service. Available at: <http://www.fao.org/ag/agl/agll/spush> (accessed on 9 September 2021).
27. USDA Natural Resources Conservation Service: Web Soil Survey. Available at: <https://websoilsurvey.nrcs.usda.gov/app/> (accessed on 15 November 2020).

28. Öztürk, Waisel, Y., Khan, M. A., & Görk, G. (2006). *Biosaline Agriculture and Salinity Tolerance in Plants* (Öztürk, Y. Waisel, M. A. Khan, & G. Görk, Eds.; 1st ed. 2006.). Birkhäuser Basel.
<https://doi.org/10.1007/3-7643-7610-4>
29. Singer, Munns, D. N., Munns, D. N., & Munns, D. N. (Donald N. (1996). *Soils : an introduction* (Third edition.). Prentice Hall.
30. R.P.C. Morgan. 2005. Soil Erosion and Conservation.
31. Rengasamy. (2010). Soil processes affecting crop production in salt-affected soils. *Functional Plant Biology : FPB*, 37(7), 613–620. <https://doi.org/10.1071/FP09249>
32. Moore, Christopher B. Edgar, Jason G. Vogel, Robert A. Washington-Allen, Rosaleen G. March, & Rebekah Zehnder. (2016). Tree mortality from an exceptional drought spanning mesic to semiarid ecoregions. *Ecological Applications*, 26(2), 602–611. <https://doi.org/10.1890/15-0330>
33. Hanson, B.R., S.R. Grattan and A. Fulton. 2006. Agricultural Salinity and Drainage. UC Davis Publication 3375.
34. Ayers, R.S. and D.W. Westcot. 1994. Water Quality for Agriculture. FAO Irrigation and Drainage Paper 29, Rev 1. ISBN 92-5-102263-1
35. Kassam. (2003). Farming Systems and Poverty 2001: Improving Farmers' Livelihoods in a Changing World. By J. Dixon, A. Gulliver and D. Gibbon. Rome and Washington DC: FAO and the World Bank (2002), pp. 412, £27.00, ISBN 92-5-104627-1 [Review of *Farming Systems and Poverty 2001: Improving Farmers' Livelihoods in a Changing World*. By J. Dixon, A. Gulliver and D. Gibbon. Rome and Washington DC: FAO and the World Bank (2002), pp. 412, £27.00, ISBN 92-5-104627-1]. *Experimental Agriculture*, 39(1), 109–110. Cambridge University Press.
<https://doi.org/10.1017/S0014479702211059>
36. Akpo, Ojiewo, C. O., Kapran, I., Omoigui, L. O., Diama, A., & Varshney, R. K. (2021). *Enhancing Smallholder Farmers' Access to Seed of Improved Legume Varieties Through Multi-Stakeholder Platforms: Learning from the TLIII Project Experiences in Sub-Saharan Africa and South Asia*. Springer Singapore Pte. Limited.

37. Jat, H. S., Datta, A., Sharma, P. C., Kumar, V., Yadav, A. K., Choudhary, M., Choudhary, V., Gathala, M. K., Sharma, D. K., Jat, M. L., Yaduvanshi, N. P. S., Singh, G., & McDonald, A. (2018). Assessing soil properties and nutrient availability under conservation agriculture practices in a reclaimed sodic soil in cereal-based systems of North-West India. *Archiv Für Acker- Und Pflanzenbau Und Bodenkunde*, 64(4), 531-545.
38. Mukhopadhyay, Sarkar, B., Jat, H. S., Sharma, P. C., & Bolan, N. S. (2021). Soil salinity under climate change: Challenges for sustainable agriculture and food security. *Journal of Environmental Management*, 280, 111736-. <https://doi.org/10.1016/j.jenvman.2020.111736>
39. Zhou, & Nguyen, H. T. (2021). *High-throughput crop phenotyping* (Zhou & H. T. Nguyen, Eds.). Springer.
40. Li, L., Zhang, Q., & Huang, D. (2014). A review of imaging techniques for plant phenotyping. *Sensors (Basel, Switzerland)*, 14(11), 20078-20111.
41. Westoby, M. J., Brasington, J., Glasser, N. F., Hambrey, M. J., & Reynolds, J. M. (2012). 'Structure-from-motion' photogrammetry: A low-cost, effective tool for geoscience applications. *Geomorphology (Amsterdam, Netherlands)*, 179, 300-314.
42. Friedli, M., Kirchgessner, N., Grieder, C., Liebisch, F., Mannale, M., & Walter, A. (2016). Terrestrial 3D laser scanning to track the increase in canopy height of both monocot and dicot crop species under field conditions. *Plant Methods*, 12(1), 9-9.
43. Liu, X., Dong, X., Xue, Q., Leskovar, D. I., Jifon, J., Butnor, J. R., & Marek, T. (2018). Ground penetrating radar (GPR) detects fine roots of agricultural crops in the field. *Plant and Soil*, 423(1), 517-531.
44. Tilly, N., Hoffmeister, D., Cao, Q., Huang, S., Lenz-Wiedemann, V., Miao, Y., Bareth, G. (2021). Multitemporal crop surface models: accurate plant height measurement and biomass estimation with terrestrial laser scanning in paddy rice. *Journal of Applied Remote Sensing*.

45. Tuyen, Lal, S. K., & Xu, D. H. (2010). Identification of a major QTL allele from wild soybean (*Glycine soja* Sieb. & Zucc.) for increasing alkaline salt tolerance in soybean. *Theoretical and Applied Genetics*, 121(2), 229–236. <https://doi.org/10.1007/s00122-010-1304-y>
46. Campbell, K. (2006). Remote sensing. *Encyclopedia of environmetrics*.
47. Calders, Adams, J., Armston, J., Bartholomeus, H., Bauwens, S., Bentley, L. P., Chave, J., Danson, F. M., Demol, M., Disney, M., Gaulton, R., Krishna Moorthy, S. M., Levick, S. R., Saarinen, N., Schaaf, C., Stovall, A., Terry, L., Wilkes, P., & Verbeeck, H. (2020). Terrestrial laser scanning in forest ecology: Expanding the horizon. *Remote Sensing of Environment*, 251(112102), 112102–. <https://doi.org/10.1016/j.rse.2020.112102>
48. Lefsky, Cohen, W. B., Parker, G. G., & Harding, D. J. (2002). Lidar Remote Sensing for Ecosystem Studies: Lidar, an emerging remote sensing technology that directly measures the three-dimensional distribution of plant canopies, can accurately estimate vegetation structural attributes and should be of particular interest to forest, landscape, and global ecologists. *Bioscience*, 52(1), 19–30. [https://doi.org/10.1641/0006-3568\(2002\)052\[0019:LRSFES\]2.0.CO;2](https://doi.org/10.1641/0006-3568(2002)052[0019:LRSFES]2.0.CO;2)
49. Eitel, J.U.H., Vierling, L.A., Long, D.S., Hunt, E.R., 2011. Early season remote sensing of wheat nitrogen status using a green scanning laser. *Agric. For. Meteorol.* 151, 1338–1345.
50. Eitel, J.U.H., Vierling, L.A., Brown, T.T., Huggins, D.R. 2014. LIDAR based biomass and crop nitrogen estimates for rapid, non-destructive assessment of wheat nitrogen status. *Field Crops Research* 159: 21-32.
51. Ehlert, D., Adamek, R., Horn, H.-J., 2009. Laser rangefinder-based measuring of crop biomass under field conditions. *Precis. Agric.* 10, 395–408.
52. Hosoi, F., Omasa, K., 2009. Estimating vertical plant area density profile and growth parameters of a wheat canopy at different growth stages using three dimensional portable lidar imaging. *ISPRS J. Photogramm. Remote Sens.* 64, 151–158.

53. Tilly, N., Hoffmeister, D., Schiedung, H., Hütt, C., Brands, J., & Bareth, G. (2014). Terrestrial laser scanning for plant height measurement and biomass estimation of maize. *International Archives of the Photogrammetry, Remote Sensing and Spatial Information Sciences.*, XL(7), 181-187.
54. Eitel, J.U.H., Long, D.S., Gessler, P.E., Hunt, E.R., Brown, D.J., 2009. Sensitivity of ground-based remote sensing estimates of wheat chlorophyll content to variation in soil reflectance. *Soil Sci. Soc. Am. J.* 73, 1715–1723.
55. Hoffmeister, Guido Waldhoff, Wolfgang Korres, Constanze Curdt, & Georg Bareth. (2016). Crop height variability detection in a single field by multi-temporal terrestrial laser scanning. *Precision Agriculture*, 17(3), 296–312. <https://doi.org/10.1007/s11119-015-9420-y>
56. Fang, Y., Qiu, X., Guo, T., Wang, Y., Cheng, T., Zhu, Y., Chen, Q., Cao, W., Yao, X., Niu, Q., Hu, Y., & Gui, L. (2020). An automatic method for counting wheat tiller number in the field with terrestrial LiDAR. *Plant Methods*, 16(1), 1-132.
57. Xiang, Bao, Y., Tang, L., Ortiz, D., & Salas-Fernandez, M. G. (2019). Automated morphological traits extraction for sorghum plants via 3D point cloud data analysis. *Computers and Electronics in Agriculture*, 162, 951–961. <https://doi.org/10.1016/j.compag.2019.05.043>
58. Zhang, Yang, Y., Zhang, Q., Duan, R., Liu, J., Qin, Y., & Wang, X. (2023). Toward Multi-Stage Phenotyping of Soybean with Multimodal UAV Sensor Data: A Comparison of Machine Learning Approaches for Leaf Area Index Estimation. *Remote Sensing (Basel, Switzerland)*, 15(1), 7–. <https://doi.org/10.3390/rs15010007>
59. Lambot, Slob, E. C., van den Bosch, I., Stockbroeckx, B., & Vanclooster, M. (2004). Modeling of ground-penetrating Radar for accurate characterization of subsurface electric properties. *IEEE Transactions on Geoscience and Remote Sensing*, 42(11), 2555–2568. <https://doi.org/10.1109/TGRS.2004.834800>
60. Huisman, Hubbard, S. S., Redman, J. D., & Annan, A. P. (2003). Measuring soil water content with ground penetrating radar; a review. *Vadose Zone Journal*, 2(4), 476–491. <https://doi.org/10.2113/2.4.476>

61. Doolittle, J. A., Minzenmayer, F. E., Waltman, S. W., Benham, E. C., Tuttle, J. W., & Peaslee, S. D. (2007). Ground-penetrating radar soil suitability map of the conterminous United States. *Geoderma*, *141*(3), 416-421.
62. Doolittle, James A.; Butnor, John R. 2009. Soils, peatlands, and biomonitoring. In: Ground Penetrating Radar: Theory and Applications, ed. Jol, Harry; Elsevier. pp 179-202. Chapter 6.
63. Al Hagrey, & Mueller, C. (2000). GPR study of pore water content and salinity in sand. *Geophysical Prospecting*, *48*(1), 63–85. <https://doi.org/10.1046/j.1365-2478.2000.00180.x>
64. Tsoflias, & Becker, M. W. (2008). Ground-penetrating-radar response to fracture-fluid salinity; why lower frequencies are favorable for resolving salinity changes. *Geophysics*, *73*(5), J25–J30. <https://doi.org/10.1190/1.2957893>
65. Grossman, & Rice, K. J. (2012). Evolution of root plasticity responses to variation in soil nutrient distribution and concentration. *Evolutionary Applications*, *5*(8), 850–857. <https://doi.org/10.1111/j.1752-4571.2012.00263.x>
66. Liu, X., Dong, X., & Leskovar, D. I. (2016). Ground penetrating radar for underground sensing in agriculture: A review. *International Agrophysics*, *30*(4), 533-543.
67. Li, Zhang, Q., & Huang, D. (2014). A review of imaging techniques for plant phenotyping. *Sensors*, *14*(11), 20078–20111. <https://doi.org/10.3390/s141120078>

CHAPTER 2

Article

Tracking the above- and belowground phenology and physiological response of *Sorghum bicolor* to highly saline-sodic soils using lidar and radar technologies in Fallon, Nevada, United States

Erin L. Smith ¹, Robert A. Washington-Allen ^{1*}, Melinda K. Yerka ¹, Alfredo Delgado ², Christopher Bernau ³, Mathew Humphrey ³, Anil Kunapareddy ⁴, Russell S. Godkin ¹, Maninder K. Walia ⁵, Uriel Cholula Rivera ⁶, Manuel A. Andrade-Rodriguez ¹ and Paul S. Verburg ⁷

¹ Department of Agriculture, Veterinary & Rangeland Science, University of Nevada, Reno, Reno, NV

² Geosystems Department, IDS GeoRadar, North America, Golden, CO

³ Great Basin Plant Materials Center, USDA Natural Resource Conservation Service, Fallon, NV

⁴ Molecular Biosciences, Interdisciplinary Graduate Program, University of Nevada, Reno, Reno, NV

⁵ Extension, College of Agriculture, Biotechnology & Natural Resources, University of Nevada, Reno, Reno, NV

⁶ Environmental Sciences, Interdisciplinary Graduate Program, University of Nevada, Reno, Reno, NV

⁷ Department of Natural Resources & Environmental Science, University of Nevada, Reno, Reno, NV

* Correspondence: rwashingtonallen@unr.edu; Tel.: +1-979-571-4330

Academic Editor: Robert A. Washington-Allen

Abstract: Saline and sodic soils are major abiotic stressors on the production of flood-irrigated crops in drylands. I conducted a crop phenotyping, remote sensing study on five genotypes of sorghum [*Sorghum bicolor* (L.) Moench], a drought and salt-tolerant crop, to assist in the molecular breeding of salt-tolerant cultivars. A control plot and a spatially heterogeneous saline-sodic treatment plot were established in Fallon, Nevada. The phenology of three-dimensional root mass from pre-planting to harvest was measured throughout the growing season using the 16-bit amplitude reflection values of the top 20cm of soil radargram from a dual-frequency (400MHz and 900MHz) ground penetrating radar system (GPR). The three-dimensional above-

ground plant structural phenology of the five genotypes was measured using a terrestrial laser scanner (TLS). Both GPR frequencies at 400MHz and 900MHz were able to detect root mass phenology in the control plot, with 900MHz providing greater detail for the amplitude measures. The GPR was able to detect changes in amplitude relative to a saline-sodic gradient that may have been due to changes in root mass phenology in the treatment plot. Of the four out of five genotypes that emerged, we found distinct variations in aboveground phenology in response to a salinity gradient. Overall, Richardson Seed's Ultra-Early Hybrid performed the best under the gradient of salinity with the highest rate of crop emergence (68% of expected), highest ratio of panicles to sorghum plants across all treatments (0.21 in medium-low, 0.88 in medium, and 0.54 in medium-high), and the greatest panicle volume (67.2%) relative to the control plot. This study found that TLS-measured height in the treatment plot for each of the four emerged genotypes was significantly influenced by different soil constituents, particularly pH, boron, HCO₃, and CO₃.

Keywords: crop phenotyping; genotype; GPR; TLS

2.1. Introduction

Drylands occupy 41.3 percent of the world's land area and are home to 2.1 billion people, many of whom are critically poor [1,2]. They are characterized by climates where mean annual evapotranspiration exceeds mean annual precipitation, high temperatures, and often the presence of salt-affected soils [3-5]. These regions are often viewed as less productive, however, they contribute 44 percent of the global crop production and have been valued at \$18 Trillion in ecosystem services [6].

Increasing temperatures, increasing aridity, and variable precipitation due to climate change are causing dryland expansion worldwide [7-9]. Furthermore, these climactic changes are causing an increase in salinization that is impacting irrigated agriculture. Salt-affected soils account for 20 percent of irrigated land globally and cause the removal of 0.3Mha to 1.5Mha of farmland from production each year [10]. As a result, annual rates of crop production do not keep up with the growing global demand for grain from a population predicted to reach 10.9 billion people by 2050 [11].

The combined pressures of increasing grain demand from a growing population, expanding drylands and variable climate, and greater demand on finite resources used in agriculture (i.e., arable land, water, and water quality sufficient for irrigation), threaten global food security [5]. Small farmers and rural communities are at a particular disadvantage, as they are often without the resources to mitigate soil salinization and lack access to sufficient irrigation water [7-9,10]. A solution to these pertinent global issues of food security is breeding cereal crops adapted to these abiotic and edaphic conditions, such as the grain *Sorghum bicolor* [12].

Sorghum bicolor is the fifth most grown cereal grain across the world; it is widely planted across drylands due to its higher tolerance to drought, heat, and salt-affected soils relative to

other cereal crops such as maize, rice, wheat, and barley [13]. This cereal grain was cultivated from wild sorghum between 8,000-4,000BCE and has since been selectively bred to develop a variety of cultivars [14,15]. The practices of selecting specific traits, such as leaf area index, biomass, yield, root depth, time to maturity, and linking those to known genetic markers is molecular breeding [12,16,17]. Molecular breeding selects specific genetic traits in various genotypes that respond best to an environmental condition, such as salt-affected soils, in order to develop cultivar varieties. These cultivars are ideally optimized to tolerate salt-affected soils and use fewer resource inputs, while still providing a substantial grain yield. It is therefore vitally important to support molecular breeding with improved methods for efficient data collection to develop sorghum cultivars specifically adapted to the abiotic stressors common in drylands.

Sodicity can cause clay particles to dissociate in solution, preventing aggregation in the soil column and leading to the development of an impermeable layer [18]. This can cause surface crusting and hard setting, resulting in shallow root penetration, inhibited germination, limited emergence, runoff, erosion, and difficulty in tilling or sowing. Soluble salts in soil inhibit plant water uptake by reducing the osmotic potential of the soil solution relative to that inside the plant root, thereby limiting the effective supply of water to the plant roots. Water absorbed by the plant carries salt ions that over time cause toxicity in plant tissue, negatively impacting net photosynthesis, metabolism, and protein synthesis [19].

Salt-affected soils include saline, sodic, and the combined saline-sodic soils, with common soluble salts including Na^+ , Ca^{2+} , Mg^{2+} , Cl^- , SO_4^{2-} , and HCO_3^- [20]. Sodic soils have a high percentage of absorbed Na^+ ions that cause structural and hydraulic properties of the soil to deteriorate. Both the sodium adsorption ratio (SAR), exchangeable sodium percentage (ESP), electrical conductivity (EC_e), and pH of saturated soil paste are used to measure the salinity and

sodicity of soils [21]. An ESP above 15 percent and a SAR above 13 percent are indicative of sodic or saline-sodic soils. A pH between 7 and 8.5 is common in saline-sodic soils, while a pH above 8.5 is common in sodic soils. Saline and saline-sodic soils characteristically have EC_e values above $4dS\ m^{-1}$, whereas sodic soils are often characterized by EC_e values below $4dS\ m^{-1}$ [22,23].

For many rural dryland farmers across the world, remediating salt-affected soils is unfeasible [24,25]. Saline soils can only be remediated by leaching salts out of the soil profile, which requires irrigation water of good quality and low solute content. However, leaching can incur secondary issues that could potentially impact groundwater and surface water quality with high solute leachate. Remediation of sodic soils requires adequate Ca^{2+} to exchange for the excess Na^+ at the rooting zone, this is typically achieved through the addition of chemical amendments, with gypsum being the most commonly used. Another option for mitigating the effects of salt is vegetal bioremediation, where root respiration produces CO_2 , releasing H^+ ions that cause Ca^{2+} to disassociate from $CaCO_3$, thus reducing soil sodicity. Vegetal bioremediation also improves infiltration, aggregate formation, and carbon sequestration [3]. However, vegetative bioremediation is often used in conjunction with other agronomic techniques to remove or reduce salts.

Some crops are better adapted to salt stress and possess mechanisms that help regulate water uptake, Na^+ exclusion, and Na^+ tissue tolerance; sorghum [*Sorghum bicolor* (L) Moench] is one of the most salt, heat, and drought tolerant cereal crops that is widely grown [26]. Vegetal bioremediation with Sordan, a kind of sorghum crop tolerant to saline and sodic conditions has been suggested [27]. It is important to utilize crop management, soil remediation, and irrigation strategies that fit the unique local environmental, political, and economic conditions of each

community. With further breeding, sorghum may have both a viable economic value as a cereal crop and as a plant used for bioremediation.

To develop salt-tolerant cultivars, it is important to identify and understand the genes responsible for these mechanisms. Molecular breeding programs seek to improve traits of interest through genomics, where genes associated with traits of interest are identified and tracked throughout the growth of the plant, through a process called crop phenotyping. It has been shown that salt tolerance is an “inheritable and quantitative trait” [28]. Crop breeders compare genotype phenotypic traits, such as leaf area index, average height, biomass, panicle density, root depth, and root mass as responses to various growing conditions. There is a lack of understanding salt-stress on sorghum at various stages of growth. High-throughput, high-resolution remote sensing technologies used in crop breeding can potentially address this problem. Remote sensing technologies can be used to study the physiological traits of cultivars developed in crop breeding programs, enabling the isolation of specific physiological and agronomic traits of significance, especially those adapted to abiotic stressors [10].

Currently, most phenotyping for molecular breeding purposes relies on visual assessment by experts and physical data collection, which can be highly labor-intensive and can introduce bias into data [29]. A lack of access to high-throughput phenotyping techniques to quantify traits related to gene-environment interactions hinders molecular breeding. High-throughput crop phenotyping is needed to select and train predictive models in genomic selection used in molecular breeding programs [29]. Emerging technologies such as GPR and TLS have the potential to be useful methods for non-destructively collecting high-resolution spatial and temporal crop data. These technologies highlight the growing importance of novel

applications of technology and non-destructive approaches to monitoring crop health and physiology.

Terrestrial laser scanning is a ground-based LiDAR (light detection and ranging) system capable of collecting highly accurate three-dimensional structural data, a feature unique to this type of remote sensing technology [30]. Terrestrial LiDAR was initially used to estimate biomass and gather structural information of forests, more recently TLS has been applied in agricultural studies, primarily to estimate aboveground biomass and to measure plant growth as a metric for plant health [31,32]. Depending on the wavelength of the TLS, other physiological characteristics and health metrics can be generated, such as plant water stress, leaf area index, leaf angle, panicle density, and rates of photosynthesis. Recently, TLS was used to estimate the number of tillers in a plot of wheat by using machine learning algorithms [33]. The development of technology for collecting these growth metrics is highly attractive, as manual measurements are tedious and expensive.

Understanding root dynamics is critical for agricultural production, resource management, and terrestrial biogeochemical cycling, making it significant for crop phenotyping. Destructive root sampling (i.e., digging up roots) is the most commonly used method for collecting root data, however, there are other non-destructive techniques such as minirhizotron and X-ray imaging technologies to collect in situ data [34]. Ground penetrating radar has been used in root characterization studies, but on a limited basis and has only in a few cases been used iteratively in a crop phenotyping study [35,36]. There is an increasing need for more root characterization studies in arid agriculture, which necessitates the expanded use of multiple frequencies in GPR applications [36]. However, GPR use is limited by soils with higher electrical conductivity, high clay contents, and high volumetric water contents. Soils such as these limit the depth of signal

and the return response. Doolittle et al. (2009) published a GPR soil suitability map of the conterminous United States which qualified saline and sodic soils as “unsuitable” [37]. To date, very little research exists on the use of GPR in saline or sodic soil conditions or for detection of pore water quality.

Consequently, in this crop phenotyping study, I used TLS and GPR, both active remote sensing technologies, to monitor above- and belowground traits of five of more than 400 genotypes of sorghum [*Sorghum bicolor* (L.) Moench] from the Sorghum Association Panel. These genotypes were planted in heterogeneous highly saline-sodic soil. My goals in this study were to quantitatively track the crop phenology of each of the five sorghum genotypes as they responded to different levels of sodicity and salinity and to test the efficacy of these technologies for high-throughput crop phenotyping. The aim was to determine which genotypes showed tolerance to salt stress and how these observable traits related to soil characteristics. Additionally, I wanted to use GPR in highly saline-sodic soil to test its ability to detect root mass over two frequencies (400MHz and 900MHz) and determine its effectiveness as a predictive tool for assessing soil characteristics such as salinity, sodicity, SAR, ESP, and cation exchange capacity. Based on the literature [36,38], I expected no detection of belowground characteristics of three-dimensional structure, phenology, and biomass using GPR under saline and sodic soil conditions, but I expected to detect changes in belowground structure, phenology, and biomass within the control plot. Moreover, I expected to detect significant differences in aboveground three-dimensional characteristics between the genotypes and between the sodic and saline soil treatments in the treatment plot using TLS technology.

2.2. Materials and Methods

2.2.1. Study Area

This paired plot experiment established a control plot (39°27'24.79" North, 118°46'39.23" West) and a treatment plot (39°27'15.89" North, 118°46'27.51" West). The study area was located at the United States Department of Agriculture Great Basin Plant Materials Center (USDA-GBPMC) at the University of Nevada, Reno's (UNR) experiment station, the Fallon Research Center (FRC) in Fallon, Nevada (Figure 2.1). The FRC was established in 1906 to conduct research on crop rotation, alkali salt toxicity, and alkali soil reclamation. The treatment plot was in a field that had traditionally suffered from high alkalinity that was managed by the USDA-GBPMC.

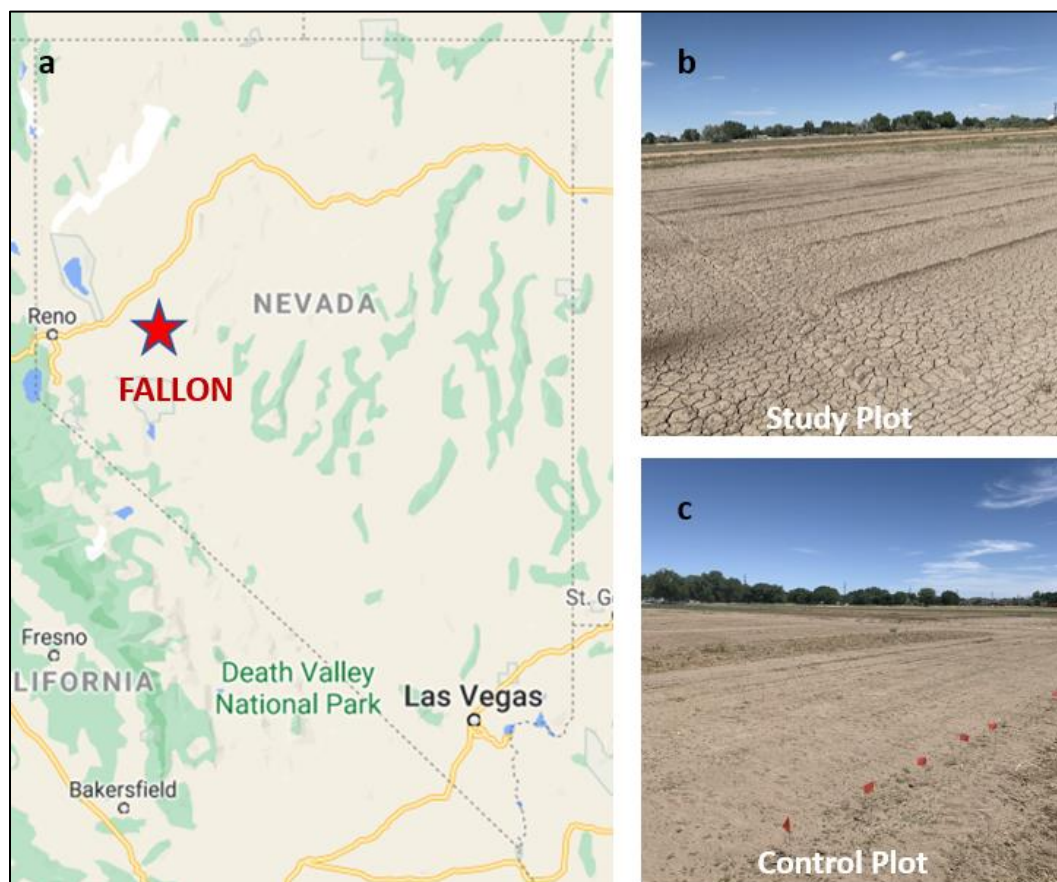


Figure 2.1. (a) Study location of the UNR FRC in Fallon, Nevada; (b) Treatment plot in June of 2020, one week prior to planting; (c) Control plot in June of 2020, one week prior to planting.

The treatment plot soil type consisted of coarse-loamy, mixed, superactive, non-acidic, mesic, oxyaquic torrifuvent [39]; soil texture was generally very fine sandy loam. The control plot was comprised of sandy, mixed, mesic, oxyaquic torrifuvent soil type, which is qualified as being prime farmland if irrigated and if factors such as soil erodibility and climate are within reasonable levels [39]; soil texture was generally loamy sand. These soil types are of the Entisol soil order and are typically found on historic stream terraces, which have parent material derived from various upgradient sources that are deposited during periodic flood events. The ecological site description of the treatment plot soil is a sodic flat (R027XY025NV – SODIC FLAT), but has the potential to be prime farmland if irrigated and reclaimed of excess salts [39]. Both plots have similar mean annual precipitation (10-15cm) and similar frost-free periods (120-140 days).

2.2.2. Trait Response to Various Soil Constituents

This study also wanted to investigate how other soil variables related to measures of salinity and sodicity and how these relationships impacted aboveground sorghum growth. Eleven soil variables were sampled across a grid in the treatment plot. These soil data were interpolated to a 2mm grid size across the treatment plot.

The control plot dimensions were 8.52m x 4.57m with five replications of one-meter rows, where each genotype was planted once in each replication, totaling 25 one-meter rows. Spacing between rows was 76cm, a common width for agriculture and wide enough to push the GPR through the rows (Figure 2.2). Prior to planting a single soil sample was collected in the center of the control plot by homogenizing four soil cores from the top 30.5cm creating a single “top soil” sample to confirm that the soil conditions were appropriate for a control plot. Additionally, TLS

target and scan positions were established at the control plot corners and mirrored in the adjacent unplanted field to the east.

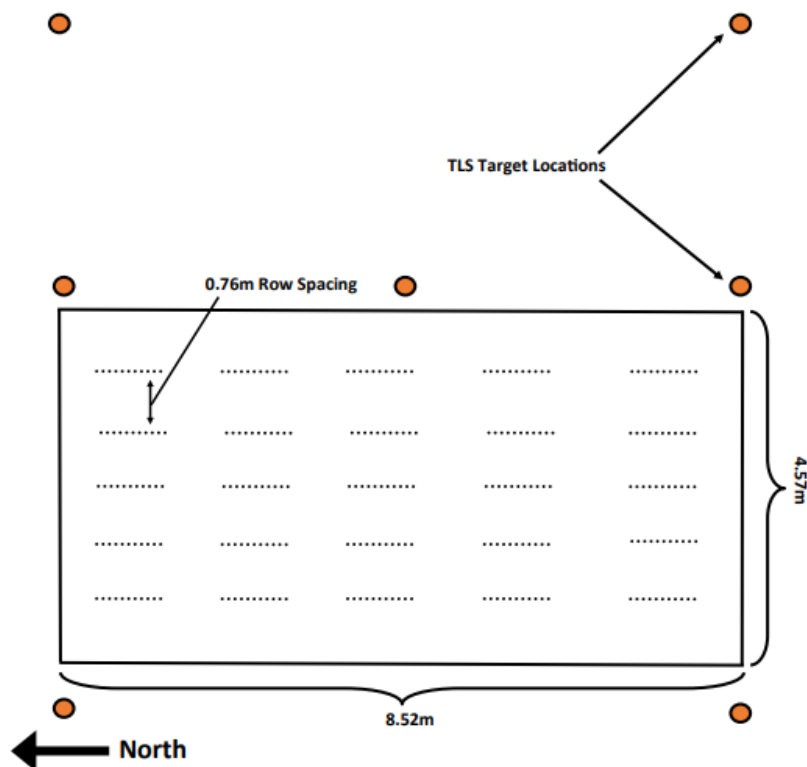


Figure 2.2. Layout of the control plot in Fallon, Nevada, with five repetitions of the five genotypes totaling 25 one-meter rows. The locations of the soil samples taken following harvest and their associated salinity concentrations, in millimolar units, are provided in the rectangles.

The treatment plot dimensions were 15.24m x 9.14m, where prior to planting soil samples were collected in a grid pattern across the plot. At each sampling point four soil cores from the top 30.5cm were collected and homogenized to create a single “top soil” sample. As a result, 15 individual replication blocks were created inside the soil sampling grid (Figure 2.3). Each replication was given a salinity treatment level based on the mean EC_e calculated by averaging the four corners. There were four salinity treatment ranges: medium-low ($8.0\text{--}9.0\text{dS m}^{-1}$), medium

(10.0-11.0dS m⁻¹), medium-high (12.0-13.0dS m⁻¹), and high (14.5-15.5dS m⁻¹). There were two medium-low replications, seven medium replications, three medium-high replications, and three high replications. The four treatment levels were intended to identify each genotype's level of tolerance to salinity; all treatment levels were considerably higher than sorghum's believed tolerance for survival [40]. All five genotypes were planted once in each replication, in one-meter rows, spaced 76cm apart, with an unplanted row called "n/a" in Figure 2.3. Additionally, TLS target and scan locations were established at each of the treatment plot corners.

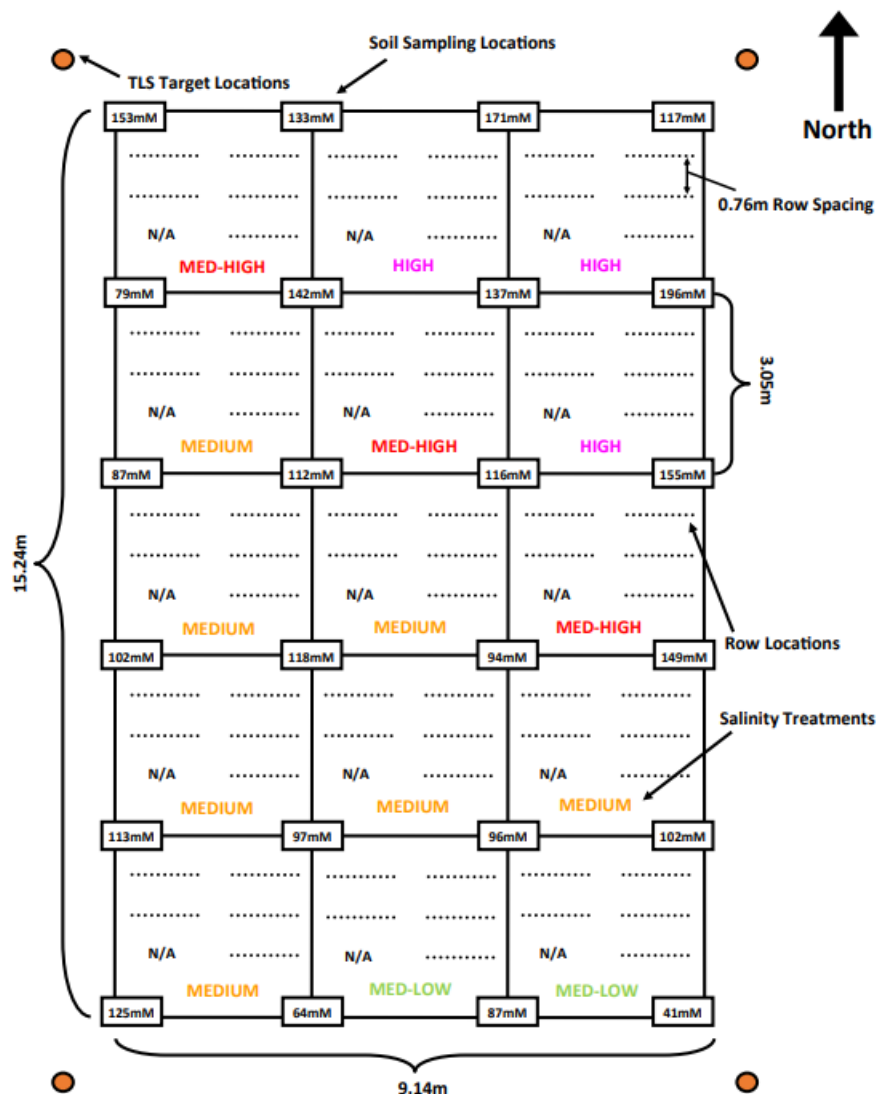


Figure 2.3. The layout of the treatment plot in Fallon, Nevada, which includes 15 replications of the five genotypes, totaling 75 one-meter rows; “n/a” represents locations where no genotypes were planted. Each replication is set up within a block design where all five genotypes are planted within each block. Furthermore, each block has relative salinity levels of medium-low, medium, medium-high, and high. Salinity levels were determined from pre-planting soil sampling. Salinity concentrations from the outside four corners of each block were averaged to get the relative salinity levels; salinity concentrations are provided in millimolar units for each sampling location across the treatment plot.

Both the control plot and treatment plot were flood irrigated with approximately 30.5cm of water every week until the sorghum plants reached full seed maturity. Water was supplied by

the Truckee-Carson Irrigation District through a network of surface irrigation ditches. Irrigation water was sourced from the Truckee River, with a diversion at the Derby Dam approximately 32km downstream of Reno, Nevada, then conveyed to the Lahontan Reservoir, and distributed through open channels for irrigation purposes. Water quality data for the control and treatment plots were not available, however, it was assumed to be similar or identical at the irrigation ditches, based on the close proximity of the two plots to each other. Following harvest, soil samples were collected in the treatment plot at the pre-planting sampling locations as a check on irrigation water quality. Similarly, soil samples were collected in a grid pattern across the control plot (12 total) to check irrigation water quality and confirm the soil composition was indeed appropriate for a control.

Aluminum flashing (5cm x 20cm strips) was buried at 15cm, 30cm, and 60cm depths within both the control and treatment plot at georeferenced locations. These were intended to be used as calibration for the GPR signal velocity.

2.2.3. *Planting*

Five separate genotypes of sorghum were selected from the Sorghum Association Panel, these included PI-533752, PI-533912, PI-533936, Richardson Seed's Ultra-Early Hybrid (Richardson), and S&W Seed Company Sordan 79 (S&W Seed). These specific genotypes were chosen based on their likelihood to be salt tolerant, which was evidenced by previous field work. Both plots utilized conventional agronomic practices for grain sorghum production. The seed beds were laser-leveled to ensure even coverage for flood irrigation. Soil preparation involved using a moldboard plow, which cuts soil and partially overturns the soil to allow for the application of soil amendments and planting of seed. Each one-meter row in the control plot and

treatment plot was hand planted with the five genotypes of sorghum. The rows were thinned throughout the growing season, as needed, to keep 8cm spacing between individual plants. Given the 8cm spacing parameter, the estimated maximum number of plants that could occupy a one-meter row is approximately 14 plants.

The treatment plot had a mean pH of 9.3, which required the addition of elemental Sulphur to be added prior to planting, to bring the pH down to 7.5 to facilitate sorghum growth. Other soil nutrients such as calcium (Ca), nitrogen (N), phosphorus (P), and potassium (K) were found to be within acceptable ranges for sorghum cultivation.

The control plot was divided into five replications running east to west, where each of the five sorghum genotypes were planted in each replication following a randomized experimental design (Figure 2.4). The five sorghum genotypes were planted within each of the replication blocks in the treatment plot in a randomized order (Figure 2.5).

← North

PI-533752	PI-533936	PI-533936	PI-533752	Richardson
S&W Seed	PI-533912	Richardson	PI-533912	S&W Seed
PI-533912	S&W Seed	S&W Seed	PI-533936	PI-533752
PI-533936	Richardson	PI-533752	Richardson	PI-533912
Richardson	PI-533752	PI-533912	S&W Seed	PI-533912

Figure 2.4. Distribution of the five genotypes in the control plot, where each replication is outlined in black. In the replication farthest to the south genotype PI-533912 was inadvertently planted twice in place of genotype PI-533936.

PI-533912	PI-533936	PI-533752	S&W Seed	Richardson	PI-533912
Richardson	PI-533752	PI-533936	Richardson	S&W Seed	PI-533912
None	S&W Seed	None	PI-533912	None	PI-533752
PI-533752	PI-533912	Richardson	S&W Seed	S&W Seed	PI-533912
Richardson	PI-533936	PI-533936	PI-533912	PI-533752	Richardson
None	S&W Seed	None	PI-533752	None	PI-533936
PI-533752	PI-533912	PI-533936	PI-533752	Richardson	PI-533912
PI-533936	Richardson	PI-533912	S&W Seed	S&W Seed	PI-533752
None	S&W Seed	None	Richardson	None	PI-533936
S&W Seed	PI-533752	S&W Seed	PI-533936	PI-533912	Richardson
Richardson	PI-533936	PI-533752	PI-533912	S&W Seed	PI-533752
None	PI-533912	None	Richardson	None	PI-533936
Richardson	S&W Seed	PI-533936	PI-533912	Richardson	S&W Seed
PI-533912	PI-533936	PI-533752	S&W Seed	PI-533936	PI-533912
None	PI-533752	None	Richardson	None	PI-533752



 North

Figure 2.5. The distribution of the five genotypes in the treatment plot where each treatment block is outlined in black and color-coded by level; medium-low is yellow, medium is light blue, medium-high is blue, and high is dark blue. Genotypes were planted in one-meter row that ran from east to west. However, here it is oriented to the north for easier viewing.

2.2.4. TLS and GPR Field Sampling

Throughout the growing season, data collection was conducted once each week until sorghum reached maturity, then every two weeks until harvest. Throughout the growing season TLS data collection was conducted 15 times and GPR data collection was conducted 16 times in both the control and treatment plots (Table 2.1). During these data collection sessions both above- and belowground data were gathered, however, there were some instances where the control plot and treatment plot scans had to be collected on different days of the same week.

Table 2.1. Schedule of data collection for the control and treatment plot in Fallon, Nevada using the TLS and GPR for the control plot and treatment plot. Except where noted, TLS and GPR scans were collected simultaneously at each plot. RMSE = root mean square error of registration.

Control Plot	Number of TLS Scans (RMSE)	Treatment Plot	Number of TLS Scans (RMSE)
May 26, 2020	4x (2.0mm)	May 27, 2020	3x (2.1mm)
June 6, 2020	4x (2.1mm)	June 8, 2020	3x (2.1mm)
June 8, 2020	4x (2.7mm)	June 18, 2020	3x (1.7mm)
June 15, 2020	5x (4.2mm)	June 25, 2020	3x (1.7mm)
June 25, 2020	5x (5.0mm)	July 2, 2020	3x (1.9mm)
July 2, 2020	5x (5.0mm)	July 16, 2020	3x (2.0mm)
July 9, 2020	5x (3.9mm)	July 22, 2020	4x (3.9mm)
July 16, 2020	5x (5.8mm)	Aug. 6, 2020	4x (2.7mm)
July 22, 2020	5x (7.1mm)	Aug. 12, 2020	4x (2.0mm)
Aug. 6, 2020	7x (8.0mm)	Aug. 18, 2020	4x (2.6mm)
Aug. 12, 2020	7x (5.9mm)	Aug. 26, 2020	4x (2.3mm)
Aug. 18, 2020	7x (5.5mm)	Sept. 2, 2020	4x (2.9mm)
Sept. 16, 2020	5x (5.3mm)	Sept. 16, 2020	4x (3.9mm)
Sept. 30, 2020	5x (6.0mm)	Sept. 30, 2020	4x (4.2mm)
Oct. 14, 2020	5x (4.7mm)	Oct. 14, 2020	4x (3.2mm)
Nov. 5, 2020	*Only GPR Scan Collected	Nov. 5, 2020	*Only GPR Scan Collected

Aboveground phenology and physiological characteristics were monitored with a FARO™ Focus3D X 330 (FARO) TLS (Table 2.2). The FARO TLS is a phase shift ground-based laser scanner that operates at 1550nm wavelength. Scans were collected from multiple angles, 360 degrees around each plot. To facilitate accurate data processing and registration of scans, white spheres were placed at the corners and edges of each plot as targets. The control plot exhibited

significant growth throughout the season, which required more frequent scans and the use of additional targets to address occlusion-related issues during data processing. A total of 73 scans for the control plot were registered to produce 15 different point clouds and 54 total scans were registered to produce 15 point clouds for the treatment plot.

Table 2.2. Equipment specifications for the FARO Focus3D X 330 terrestrial laser scanner, used in this study to collect aboveground phenotypic characteristics.

TLS Parameter	Scan Preset Values
Wavelength	Infra-red 1550nm
Range	0.6m to 330m
Scan Size (pts)	10,240 x 4,410
Resolution (Mpts)	45.2 (1/4)
Field-of-View	Horizontal: 0.0 to 260.0 degrees Vertical: -60.0 to 90.0 degrees
Beam Divergence	0.19mrad (0.011 degrees)

Belowground root monitoring and data collection were conducted using an IDS GeoRadar RIS MF Hi-Mod Dual-channel (IDS GeoRadar) ground penetrating radar, which was equipped with a custom three-dimensional printed carriage and integrated with an Emlid Reach RS2 real-time-kinematic global positioning system (GPS). The OneVision software from IDS GeoRadar was used for data collection in the field, allowing for real-time viewing of the RADAR image, or rardargrams. The GPR was equipped with two antennas to transmit and receive at 400MHz and 900MHz frequency. Polarization was adjustable and was set to horizontal (transmitted) and horizontal (received), or HH polarization (Table 2.3).

Table 2.3. The specifications of the IDS GeoRadar RIS MF Hi-Mod Dual-channel ground penetrating radar system that was used in this study.

GPR Parameter	Value
Footprint	38cm x 43cm (Single antenna)
Channels	2 (up to 8)
Frequency	400MHz / 900MHz
Polarization	Horizontal (HH)
Antenna Spacing	50cm

Biomass samples were collected in both the control plot and treatment plot on October 30th, 2020, prior to harvesting, when the plants had reached maturity and had fully dried-down in the field. Samples were collected where available throughout the treatment plot; samples were collected in each of the treatments and for the four genotypes that emerged. When possible, plants with seedheads were chosen for sample collection. Due to the data collection needs for other studies and the limited aboveground biomass that grew in the treatment plot, limited samples were collected. Two individual plants, both above- and belowground biomass, were collected for each genotype in the control plot. These biomass samples were used to validate remote sensing data.

2.2.5. TLS Data Processing and Analysis

After each data collection event, field data from the TLS individual scans were registered together into a single point cloud using FARO SCENE, a proprietary software [41]. Point clouds were exported from FARO SCENE software as LAS files, then stray points and ground points were removed, and genotypes were segmented by treatment in CloudCompare [42], an opensource software for point cloud processing (Figure 2.6 a-c). Clipping 15 point clouds and

25 individual one-meter rows amounted to a total of 375 aboveground analytical units for the control plot; 15 point clouds and 90 individual one-meter rows totaled 1,350 aboveground analytical units for the treatment plot. Analytical units were used to track individual genotype response to treatments and to capture trait phenology.

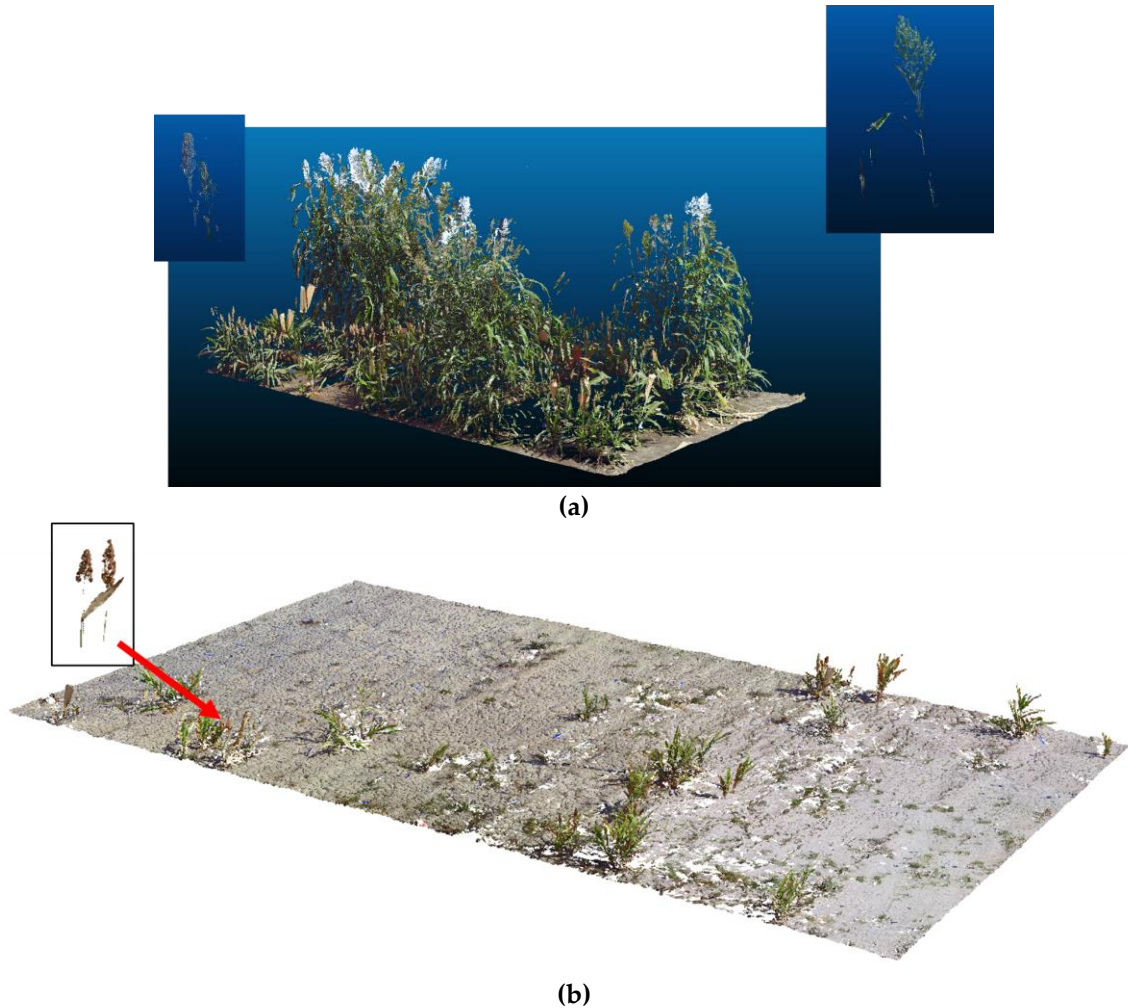


Figure 2.6. (a) A colorized TLS point cloud of the control plot at maturity (September 30, 2020), with examples of individual panicles segmented (insets); (b) Colorized TLS point cloud of the treatment plot at maturity (September 30, 2020), clipped to plot-scale and panicle segmented (inset).

Clipped point clouds were rasterized in QGIS, an opensource software, to 5cm pixel size [43]. This pixel size was chosen as a conservative grid size, considering point cloud registration in FARO SCENE software had a mean point error that ranged from 1.7 to 8.0mm. The 5cm pixel resolution was sufficient to capture individual parts of a single sorghum plant throughout its growth. Rasters were georeferenced in QGIS and overlaid with a template that identified individual rows. This template allowed for the comparison of unique row data with below-ground data. The resulting data was exported in comma-separated variable format and analyzed using RStudio [44], an open-source software. Figure 2.7 provides the general workflow for TLS data processing.

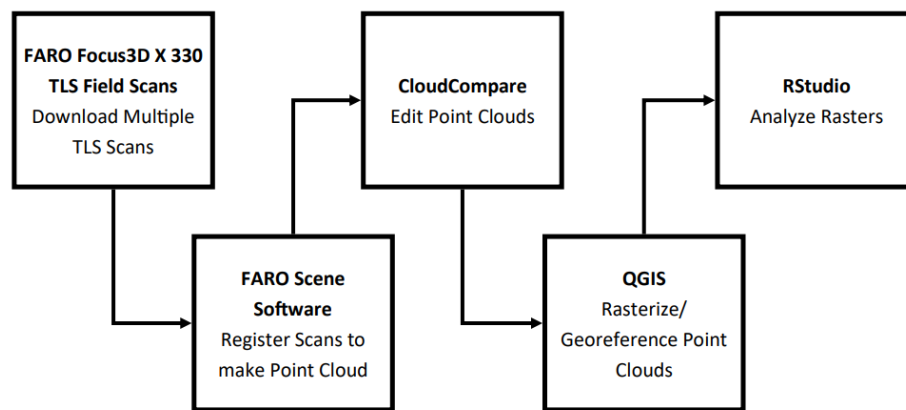


Figure 2.7. Workflow diagram for TLS data processing for aboveground phenology in the control and treatment plots for this study.

Other programs were tried for ground removal, these included Quick Terrain Modeler, Surfer, and RStudio, however, they were not as effective as CloudCompare and often removed five to ten centimeters of the aboveground biomass from the treatment plot. Due to the need for a high level of detail for continued analysis, especially in the treatment plot where aboveground biomass was substantially lower than the control plot, point cloud clipping in CloudCompare was found to be more suitable.

2.2.6. GPR Data Processing and Analysis

Ground penetrating radar data collected in the field was processed using GPR-SLICE© software, which may have facilitated root visualization and seasonal root growth measurements. Georeferenced GPR data from the IDS GeoRadar unit was downloaded, but before processing, the raw SCAN files needed to be converted to the DT file format used by GPR-SLICE.

Depth calibration required estimating velocity based on the known root depths observed during biomass collection as the aluminum flashing was not detected in GPR SLICE but was detectable in real-time viewing of OneVision. However, velocity estimation was only used in the control plot, as it had an even conductivity reading across the entire plot (approximately 0.8dS m^{-1}). In contrast, the treatment plot had significant changes in soil conductivity, which could cause apparent reflected depths to vary [45]. Consequently, only the top 20cm of the radar return signal was utilized for the analysis in the treatment plot.

Within GPR-SLICE, a time zero correction was made for each scan to remove air waves from ground wave reflections. This was achieved by using the software option for a 15 percent threshold detection for the return amplitude, which was performed line-by-line for each scan. Subsequently, a bandpass filter was applied to select specific ranges, effectively reducing drift in the data. For the 900MHz frequency, a range of 450-1350MHz was used, and for the 400MHz frequency, a range of 200-600MHz was chosen, these were based on power spectra return responses. A Hilbert transform was then applied to enhance the amplitude response of root masses, making them more detectable when converted to a raster file format.

After filtering, the radargrams were sliced at an approximate depth of 30cm for the control plot and 20cm for the treatment plot. These depths were based from the known mean

root mass depth, observed during physical biomass collection. The amplitude response for each slice was inverse distance weighted and gridded with a small search radius, with grid cells set to five centimeters. The resulting gridded slices were exported from GPR-SLICE© as georeferenced GRD files. The return amplitude responses were further analyzed in QGIS by overlaying a template with the locations of each row by genotype and treatment block. The data was then extracted from QGIS and analyzed in R Studio for further analysis and interpretation. A general workflow for GPR data processing and analysis is provided in Figure 2.8.

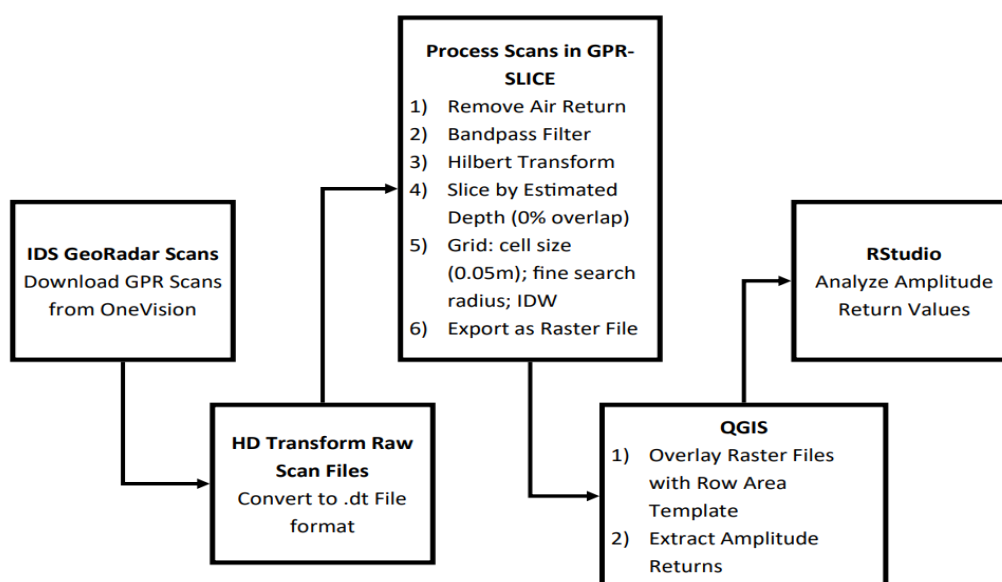


Figure 2.8. Workflow for GPR data processing for monitoring of root response in the control and treatment plots.

Errors with the RTK GPS unit for the GPR scans resulted in the removal from analysis of scans one through six for the control plot and scans one through five for the treatment plot. The remaining 10 scans for the control plot, which were segmented by the 25 one-meter rows, totaled 250 belowground analytical units. For the treatment plot, the remaining 11 scans were segmented by the 90 one-meter rows, which totaled 990 belowground analytical units.

2.3. Results

2.3.1. Aboveground Phenology and Response to Treatments

Only four of the five genotypes emerged in the treatment plot, these were: PI-533752, PI-533912, Richardson, and S&W Seed. Additionally, there was no emergence in the high salinity treatment from any genotype. The aboveground height phenology of all five genotypes is provided in Figure 2.9, which compares the phenology of each genotype in response to the saline-sodic gradient to that of the control plot, as the mean of the maximum row heights.

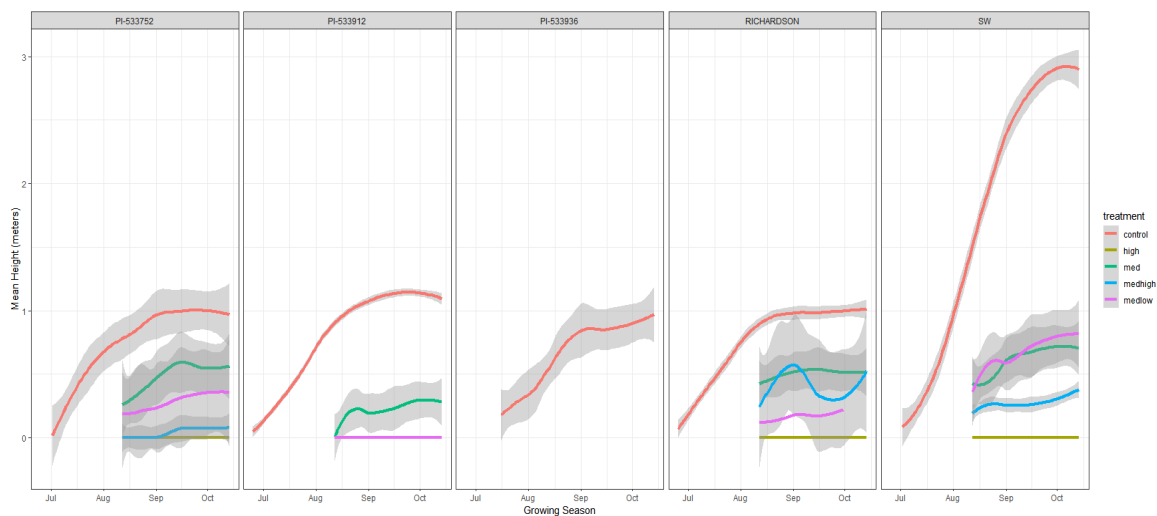


Figure 2.9. Plotting the treatment plot treatments next to the control plot phenology for each of the five genotypes, with mean height in meters on the y-axis and growing season on the x-axis. The 95 percent confidence interval for mean height shades the area around each growth curve.

The height of each genotype relative to the control plot was analyzed for each treatment and is given as a percentage of the control plot mean height (Table 2.4). These height data were taken on September 30, 2020 from TLS LiDAR point clouds when all sorghum plants had reached either maturity or their maximum aboveground growth, some plants never reached maturity in

the treatment plot. A Chi-squared test was performed on the heights as percent of control for each genotype and by treatment (Table 2.5).

Table 2.4. Mean heights of each sorghum genotype at maturity on September 30, 2020 are given in centimeters for each salinity treatment, and as a proportion of their mean heights in the control plot (provided as a percentage). Height data was analyzed from TLS LiDAR point clouds.

GENOTYPE	Med-Low (% of Control)	Medium (% of Control)	Med-High (% of Control)	Control
Richardson	23.4cm (23.0%)	46.7cm (45.9%)	32.0cm (31.4%)	101.8cm (100%)
S&W Seed	84.9cm (27.8%)	78.9cm (25.8%)	43.9cm (14.4%)	305.4cm (100%)
P-533912	0.0cm (0.0%)	19.4cm (17.7%)	0.0cm (0.0%)	109.5cm (100%)
PI-533752	39.4cm (42.4%)	56.2cm (60.5%)	9.70cm (10.4%)	92.9cm (100%)
PI-533936	0.0cm (0.0%)	0.0cm (0.0%)	0.0cm (0.0%)	99.0cm (100%)

Table 2.5. Results of the Chi-squared test of the mean heights of each genotype by treatment as a percentage of the control plot mean heights to determine significant difference. Where the expected result for each treatment is 100 percent. Degrees of freedom are calculated from the number of replication in each treatment.

Treatment	Richardson	S&W Seed	PI-533912	PI-533752	PI-533936	DF (n-1)	alpha
Med-Low	157.91	160.80	200	145.20	200	1	0.05
Medium	270.41	482.03	536.98	361.37	700	6	0.05
Med-High	213.40	247.57	300	281.13	300	2	0.05
High	300	300	300	300	300	2	0.05

2.3.2. Height Response to Various Soil Constituents

The eleven soil variables were interpolated to a 2mm grid size across the treatment plot and compared using a correlation matrix (Figure 2.10).

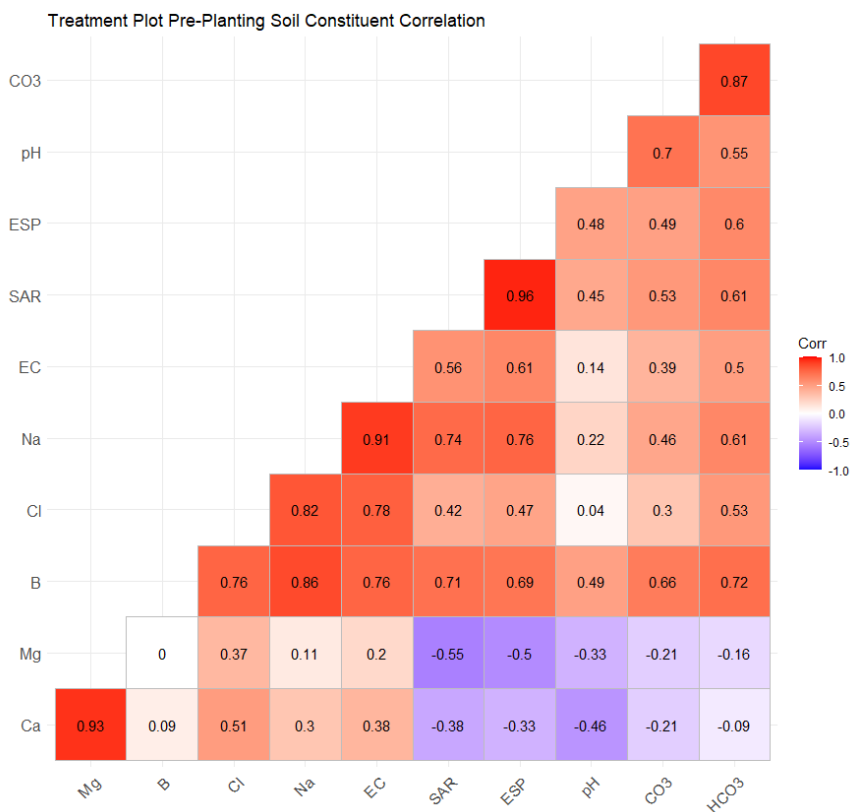


Figure 2.10. The correlation matrix shows the relationship of soil constituents for the entire treatment plot, using soil samples collected prior to planting.

Following the soils correlation matrix, a generalized linear model (GLM) regression was used to analyze potential relationships between genotype heights as a percentage of the control and a variety of soil constituents that included salinity and sodicity (Table 2.6). GLMs with p-values less than 0.05 were considered significant and were confirmed to be more significant than other models by using an Akaike Information Criterion (AIC) table. A Shapiro-Wilks test for normality was run on the model residuals for those GLMs with p-values less than 0.05 (Table 2.7). Input data for the GLM included: 1) Mean soil constituent values, from the area surrounding each one-meter row (soils data interpolated to a 2mm pixel size); 2) maximum row heights from

TLS LiDAR point clouds (rasterized to 5cm pixel size). If there was no emergence in a row, then the height for that row was zero. This data set included all treatments and all rows.

Table 2.6. Summary table of generalized linear models of soil constituents as a predictor of genotype height relative to the control plot height. P-values below 0.05 are highlighted in bold to denote significance.

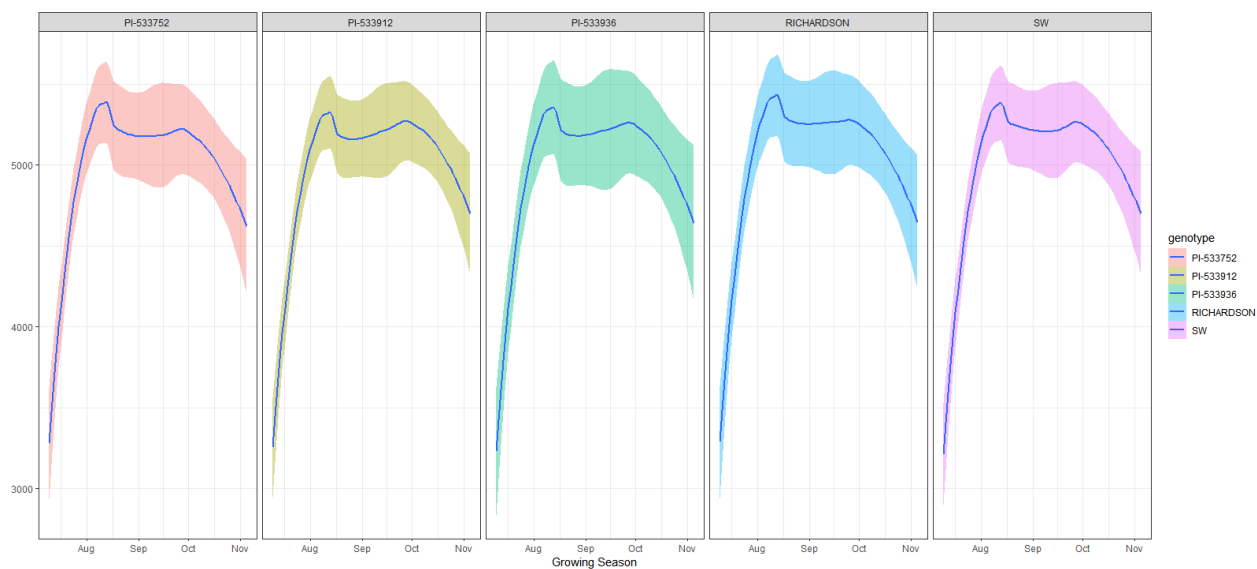
SOIL VARIABLE	PI-533752	PI-533912	Richardson	S&W Seed
	P-value (R ²)	P-value (R ²)	P-value (R ²)	P-value (R ²)
SAR	0.431 (0.04836)	0.1756 (0.1363)	0.2684 (0.09325)	0.03237 (0.3062)
pH	0.1559 (0.146)	0.7917 (0.00556)	0.0007419 (0.5963)	0.02451 (0.3322)
Na	0.1382 (0.161)	0.1835 (0.1318)	0.04305 (0.2788)	0.0441 (0.2765)
Mg	0.3702 (0.06216)	0.9101 (0.001019)	0.06333 (0.2407)	0.8379 (0.00334)
HCO ₃	0.1284 (0.1686)	0.3418 (0.06967)	0.009479 (0.4155)	0.003792 (0.4875)
ESP	0.4515 (0.04431)	0.2348 (0.1067)	0.3436 (0.06918)	0.03551 (0.2974)
EC	0.2631 (0.09521)	0.323 (0.0751)	0.0277 (0.3209)	0.1581 (0.1471)
CO ₃	0.03301 (0.3043)	0.9323 (0.0005763)	0.005805 (0.4551)	0.02749 (0.3216)
Cl	0.2199 (0.1133)	0.258 (0.09707)	0.08061 (0.2164)	0.05596 (0.253)
Ca	0.3171 (0.07686)	0.7765 (0.00642)	0.0533 (0.2579)	0.943 (0.0004093)
B	0.0377 (0.2916)	0.2879 (0.08629)	0.02075 (0.3474)	0.03695 (0.2936)

Table 2.7. Shapiro-Wilks Test for normality of model residuals for significant soil variables for each genotype. P-values equal to or lower than 0.05 for the Shapiro-Wilks Test indicate that model residuals are not normally distributed.

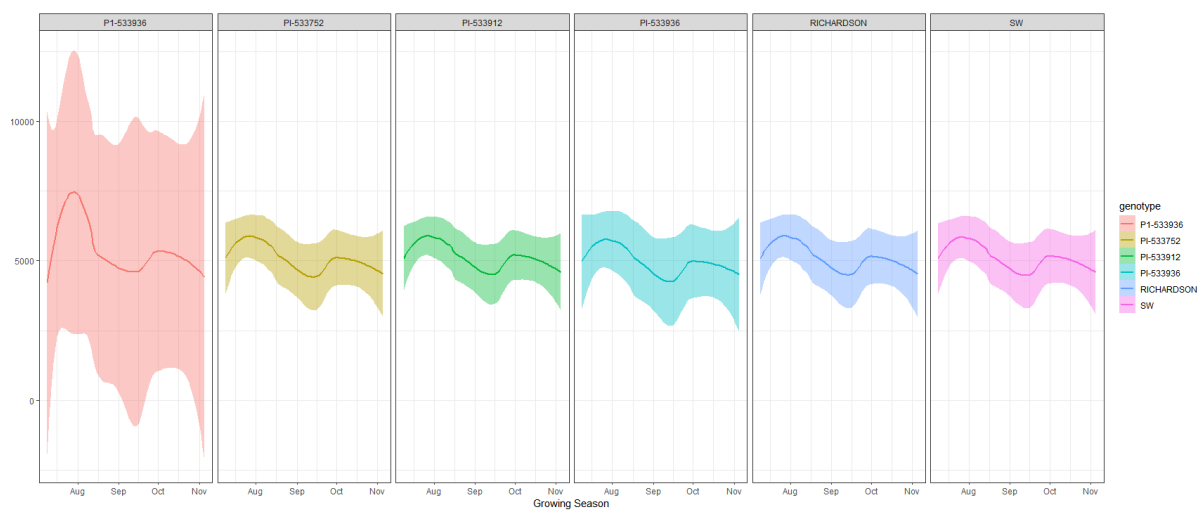
Genotype	Soil Variable	Shapiro-Wilks P-value
PI-533752	CO ₃	0.1130
	B	0.1669
PI-533912	<i>*No statistically significant soil predictor variable</i>	
Richardson	pH	0.7121
S&W Seed	HCO ₃	0.9303

2.3.3. Belowground Phenology and Response to Treatments

Root phenology was detected with the 400MHz and 900MHz GPR frequencies in the control plot with increasing return amplitude through the growing season (Figure 2.11).



(a)



(b)

Figure 2.11 a) Root phenology of the control and treatment plot showing return amplitude on the y-axis from the 400MHz frequency of the GPR; b) Root phenology of the control and treatment plot showing return amplitude on the y-axis from the 900MHz frequency of the GPR.

To determine if there is a root response in the treatment plot, the signal response from the unplanted rows was regressed to the genotypes in each salinity treatment for both the 400MHz signal return (Table 2.8) and the 900MHz return signal (Table 2.9).

Table 2.8. Regression of the 400MHz signal response of the unplanted rows in the salinity treatments to each genotype. P-values of less than 0.05 show highly correlated signal response. P-values less than 0.05 are highlighted in bold.

Genotype	Med-Low		Medium		Med-High		High	
	P-value	R ²	P-value	R ²	P-value	R ²	P-value	R ²
Richardson	0.1865	0.08573	2e-16	0.942	0.5584	0.01116	0.1603	0.06259
PI-533912	0.3006	0.05344	2e-16	0.9673	0.5845	0.009756	0.2065	0.05096
S&W Seed	7.069e-05	0.5543	2e-16	0.9561	9.72e-09	0.6593	6.804e-11	0.7517
PI-533752	0.3151	0.05042	2e-16	0.9803	0.555	0.01134	0.2092	0.05037
PI-533936	0.2456	0.06676	2e-16	0.964	0.392	0.02376	0.028	0.03753

Table 2.9. Regression of the 900MHz signal response of the unplanted rows in the salinity treatments to each genotype. P-values of less than 0.05 show highly correlated signal response. P-values less than 0.05 are highlighted in bold.

Genotype	Med-Low		Medium		Med-High		High	
	P-value	R ²	P-value	R ²	P-value	R ²	P-value	R ²
Richardson	0.178	0.1104	0.01568	0.09198	0.2431	0.05407	0.3648	0.03295
PI-533912	0.1832	0.1079	0.01534	0.09256	0.2926	0.0442	0.31	0.04118
S&W Seed	2.2e-16	0.989	2.2e-16	0.9881	2.2e-16	0.998	2.2e-16	0.9955
PI-533752	0.1856	0.1068	0.02111	0.08414	0.2664	0.04915	0.2968	0.04344
PI-533936	0.1752	0.1117	0.01764	0.08887	0.2244	0.05845	0.332	0.03768

2.3.4. Biomass Response to Treatments

The survivability rate was calculated for each row in the Treatment plot by dividing the number of plants growing in each row by the possible number of plants for a row (Table 2.10); the possible number of plants for each row was 14 given the 8cm spacing. The number of plants emerged for each genotype by treatment was analyzed with a Chi-squared test that assumed an anticipated emergence of 14 plants in each row.

Table 2.10. Survivability rate for each genotype in the Treatment plot, based on the potential possible number of sorghum plants that could exist in each row. A total number of approximately 14 plants could exist in each row.

Genotype	Med-Low (2 replications)		Medium (7 replications)		Med-High (3 replications)	
	No. Plants	Growth Rate	No. Plants	Growth Rate	No. Plants	Growth Rate
Richardson	19	68%	33	34%	13	31%
PI-533912	0	0.0%	10	10%	0	0.0%
S&W Seed	2	7.1%	33	34%	11	26%
PI-533752	2	7.1%	13	13%	1	2.4%

Table 2.11. A summary of the Chi-squared test analyzing emergence with the anticipated emergence of 14 plants for each row. Chi-squared values in bold signify an insignificant difference between actual emergence and anticipated emergence. Degrees of freedom are calculated from the number of repetitions in each salinity treatment.

Treatment	Richardson	S&W Seed	PI-533912	PI-533752	DF (n-1)	alpha
Med-Low	2.93	24.29	28	24.29	1	0.05
Medium	44.5	49.07	80.43	74.79	6	0.05
Med-High	22.07	24.21	42	40.07	2	0.05

The number of panicles produced in each of the planted rows in the treatment plot was manually verified on September 30, 2020, and data are presented in Table 2.12. In the control plot, point clouds were filtered to have an even point density to determine and average point counts for panicles in the treatment plot were regressed to mean panicle weight collected in the field (Figure 2.12). P-values of this regression are (0.03 for mean panicle mass to point count) and (0.01 for mean total panicle mass to point count).

Table 2.12. Panicle production ratio for each genotype by salinity treatment.

Genotype	Med-Low (2 rows each genotype)		Medium (7 rows each genotype)		Med-High (3 rows each genotype)	
	No. Panicles	Ratio of Panicles per Plant	No. Panicles	Ratio of Panicles per Plant	No. Panicles	Ratio of Panicles per Plant
Richardson	4	0.21	29	0.88	7	0.54
PI-533912	0	0.0	8	0.80	0	0.0
S&W Seed	0	0.0	18	0.55	0	0.0
PI-533752	0	0.0	2	0.15	0	0.0

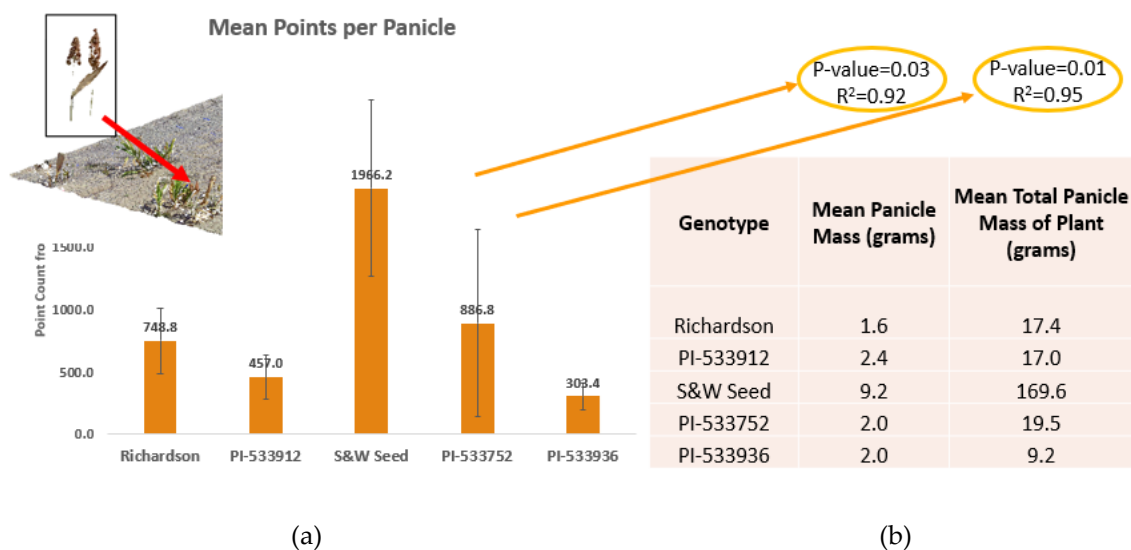


Figure 2.12. a) Mean panicle point counts from 3-D point cloud of September 30, 2020, scan of the control plot. Point density was homogenized and panicles were dissected from the point cloud; b) Regressed mean panicle point count by genotype to mean panicle mass and mean total panicle mass of sorghum plant by genotype.

2.3.5. Manually Collected Biomass

Aboveground and belowground biomass samples were collected when both plots had reached full maturity and had dried down in the field. The mean dry weight in grams of the above- and belowground biomass from samples collected in the salinity treatments and the control plot are provided in Table 2.13. These values are then converted to a ratio of above to belowground biomass for the salinity treatments and the control plot (Table 2.14).

Table 2.13. Results of the manually collected biomass samples from the salinity treatments and control plot, reported in grams. Asterisks represent where data was not collected but plants were known to grow; “n/a” represents where there was no emergence.

Genotype	Med-Low		Medium		Med-High		Control	
	Above	Below	Above	Below	Above	Below	Above	Below
Richardson	2.0	0.7	26.2	15.3	1.6	0.4	104.4	107.0

PI-533912	n/a	n/a	3.1	0.6	n/a	n/a	115.8	61.5
S&W Seed	38.2	10.8	18.5	9.4	2.9	0.7	893.7	209.8
PI-533752	***	***	14.6	4.8	***	***	129.6	103.3
PI-533936	n/a	n/a	n/a	n/a	n/a	n/a	61.2	34.1

Table 2.14. Ratio of mean aboveground biomass to mean belowground biomass. Asterisks represent missing data due to limited sample availability; “n/a” represents areas where there was no emergence.

Genotype	Control	Med-Low	Medium	Med-High
Richardson	1.0	3.7	2.8	4.1
PI 533912	1.9	n/a	5.2	n/a
S&W Seed	4.2	3.5	3.6	3.1
PI 533752	1.3	***	3.2	***
PI 533936	1.7	n/a	n/a	n/a

2.4. Discussion

2.4.1. Aboveground Sorghum Response to Salinity Treatments

In this study, when the control plot phenology of each genotype is compared to the salinity treatments it is apparent that all treatments decreased the mean maximum height of each of the four genotypes. The TLS was able to detect aboveground phenology of the five genotypes of sorghum with accuracy corroborated by observation and manual data collection. The aboveground growth in response to the four salinity treatments was significantly inhibited compared to growth in the control plot. Additionally, only four of the five sorghum genotypes were able to grow in the treatment plot (i.e., PI-533912, PI-533752, Richardson, and S&W Seed), genotype PI-533936 did not emerge in any salinity treatment. Finally, no sorghum genotypes

were able to grow in the high salinity treatment. The results of the Chi-squared test indicate that genotypes in each treatment were significantly different in mean height from the control plot mean height using an alpha level of significance of 0.05 (Table 2.5). The S&W Seed genotype had the tallest mean height in the control plot (3.05m), but the Richardson genotype was the quickest to reach maturity in early August.

In general, the height of all genotypes was significantly impacted by salinity treatment. However, the Richardson Seed's Ultra-Early Hybrid grew the most consistently across the medium-low, medium, and medium-high gradients, where height as a percentage of the control was 23.0%, 45.9%, and 31.4%, respectively. The PI-533752 genotype attained the highest percentage of its control height at 60.5% in the medium treatment; following that are S&W Seed Sordan 79, and PI-533912. Contrary to the hypothesis, salinity was not the most significant factor influencing height, rather these factors varied by genotype. The AIC table model comparison for PI-533752 confirms that CO₃ and B are most influential to percent of control height. The AIC table has a delta of 2.40 between B and HCO₃ which indicates the first two models (CO₃ and B) are significant, and model residuals are normally distributed (Shapiro-Wilks p-values = 0.113 and 0.1669, respectively). For genotype PI-533912 the AIC table model comparison indicated that there was no clear model that was more influential to predicting percent of control height. The AIC table delta values were significantly less than a value of two between models. For the Richardson genotype, the AIC table model comparison clearly indicated that pH was the most significant predictor with a delta value of 4.50 between pH and CO₃. Additionally, the pH model was normally distributed (Shapiro-Wilks p-value = 0.7121). Finally, S&W Seed Sordan 79 AIC table model comparison showed HCO₃ as the most significant predictor of percent of control height with a delta value of 3.97 between HCO₃ and pH. The model residuals were normally

distributed (Shapiro-Wilks p-value = 0.9303). Using the percent of control produced much clearer results than using the maximum row height. Each genotype had obvious soil variables affecting the percent of control height, with the exception of PI-533912.

2.4.2. Belowground Root Monitoring and Response

The return responses from the control plot varied substantially from the return responses across the four salinity treatments. In the control plot, both frequencies followed a similar trend, which is an increase in amplitude at the end of July to the beginning of August, then a gentle decrease toward the end of August followed by a slight increase in amplitudes at the beginning of October (Fig. 2.11). The return response for both the 400MHz and 900MHz frequencies across the treatment plot did not follow similar trends across the growing season. There were no steep growth curves in return amplitudes attributed to greater signal attenuation from increasing root water as was apparent with the control plot. Root phenology was detected with both the 400MHz and 900MHz frequencies in the control plot, as evidenced by the increase in return amplitudes for each genotype as plants grew toward maturity, then decreased as roots dried out nearing harvest. Both frequencies had similar patterns across the growing season in the control plot. However, the general trend in the treatment plot is that the 900MHz amplitude responses spiked once in mid-September, whereas the 400MHz amplitude responses spiked in the beginning of August and again in mid-September. Conversely, in the control plot, both frequencies increased in amplitude at the end of July to beginning of August, then a gentle decrease toward the end of August followed by a slight increase in amplitudes in the beginning of October.

Data from the 2020 study in Fallon, Nevada suggest that GPR in the 400MHz and 900MHz frequencies has limited use for identifying fine root mass in highly saline-sodic soil

conditions. Belowground imaging results throughout the growing season showed varied “mass” locations throughout the treatment plot that were unsubstantiated when compared to actual plant locations and excavated root sampling data. High soil sodicity in the treatment plot caused the deflocculation of soil aggregates that impaired drainage and caused irrigation water to sit in the upper part of the soil profile. It is unclear whether the greater issue with GPR ranging in the treatment plot came from the high relative permittivity of the soil or the lack of adequate drainage through the soil profile.

This study does suggest that GPR can detect a gradient response to soil conductivity. Returned amplitude values from genotypes in the control plot were regressed to the unplanted row within each treatment. Although the GPR was unable to significantly detect root mass, a pattern emerged between the two frequencies. There was a strong correlation in the medium salinity treatment with correlation becoming less as salinity increases.

2.4.3. Biomass Response to Salinity Treatments

Results of the Chi-squared test indicated that all rates of emergence were significantly different from the anticipated rate, except for the Richardson genotype growing in the medium-low salinity treatment (Table 2.11). The Richardson genotype had the highest rate of survivability, or mean number of plants per row relative to the expected number of 14 plants per row. Richardson produced the highest mean number of plants per row, which was represented as a percent of the expected outcome (68% in medium-low, 34% in medium, and 31% in medium-high). S&W Seed had the second highest rate of plant production (7.1% in medium-low, 34% in medium, and 26% in medium-high).

The rate of plant growth was lower in the medium salinity treatment level. However, the rate of panicle production was higher. The rate of panicle production, or ratio of panicles to plants was overall highest in the medium salinity treatment, however, Richardson had the highest ratio across all treatments, (0.21 in medium-low, 0.88 in medium, and 0.54 in medium-high). PI-533912 had the second highest panicle to plant ratio of 0.80 in the medium treatment.

Belowground biomass in the treatment plot was smaller than in the control plot. This was true for all genotypes, with the exception of PI-533936, which did not successfully grow in the treatment plot. Sample collection was limited, and not all genotypes were represented in treatments where there was indeed growth; this was due to limited sample availability. However, the Richardson genotype had the highest relative root mass accumulation within the medium salinity treatment. S&W Seed and PI-533752 had similar outcomes for root mass accumulation in the medium salinity treatment. Root mass accumulation was very limited in the medium-high salinity treatment, only Richardson and S&W Seed grew, but had root masses of less than one percent of the corresponding root masses in the control plot.

The ratio of mean above- to below-ground mass increased substantially in response to the salinity gradient when compared to the control. This was counter to the original hypothesis that excess sodium would limit water intake and induce greater root production. Most of the genotypes in the control plot had a lower ratio of less than 2:1, with the exception being the S&W Seed genotype, which had a ratio of 4.2:1. In the various salinity treatments the ratio of above- to belowground mass increased, the exception again being S&W Seed, which decreased.

2.5. Consideration for Further Study

2.5.1. Terrestrial Laser Scanning

New methods for above and belowground biomass monitoring in crop breeding was proposed for this study. In monitoring height, terrestrial laser scanning has proven to be a valuable tool in monitoring aboveground phenology in many crop phenotyping studies [32,46,47]. Its non-destructive sampling and real-time data collection capabilities make it useful for vegetation monitoring in both natural and agricultural systems. Ultimately, the use of TLS in agriculture and crop breeding studies is of particular usefulness for precision agriculture [48].

The five genotypes of sorghum used in the 2020 Fallon, Nevada salinity-sodicity study were planted in one-meter rows in a randomized plot design. In the control plot, rows were spaced 76 cm apart. At maturity, the sorghum leaves grew into one another, making the task of sectioning out each genotype in TLS point clouds difficult. Terrestrial laser scanning has been used in many agricultural applications where there is a single crop or a field with adjacent rows of the same species or genotype, but no TLS studies have been specifically developed for molecular breeding purposes.

Molecular breeding programs often grow dozens to hundreds of different genotypes each season. Molecular breeding studies comparing multiple genotype responses to environmental variables are often limited by seed quantity. Planting numerous rows of each genotype being studied may not be feasible, limiting the amount of destructive sampling that is possible and making crop phenotyping, biomass, and yield data more difficult to obtain. The industry standard for row width is 76cm, which provides enough room for sorghum to grow but results in thick leaf overlap when the crop becomes mature.

The smaller aboveground biomass produced in the treatment plot was difficult for the TLS to detect initially. In the treatment plot, aboveground growth was detectable in the TLS-generated point clouds a month after sorghum growth was apparent in field observations. The

slower rate of emergence and substantially smaller size of growth was challenging for the TLS to detect initially. Furthermore, many of the panicles that formed in the treatment plot were very small and more challenging to detect with the TLS despite increasing the number of scans collected during each sampling event.

Narrow row spacing resulted in significant areas of occlusion in the TLS point clouds, this issue was exacerbated when trying to differentiate between rows where different genotypes were planted. Significant occlusion becomes an issue of greater concern in multi-genotype studies as it can prevent accurate estimation of biomass, panicle count and density, height, and plant architecture traits. In many agricultural studies seeking height estimates or tiller counts, a TLS is rigged to either run transects above a field using cables or is placed on towers at set locations throughout the field, well above the maximum canopy height. Occlusion may be reduced in future studies by keeping the TLS sensor well above the canopy height for better line of sight to more surfaces, and more scanning angles can also improve the issue of occlusion. Terrestrial laser scanning in conjunction with LiDAR-mounted unmanned aerial vehicles (UAV) is a promising area of emerging research that may reduce occlusion and improve resolution [49]. The precision of high-resolution, georeferenced LiDAR data with new methods for individual genotype and even individual plant detection is the future of genotype-based molecular breeding studies.

2.5.2. Ground Penetrating Radar

Root detection and monitoring is important for estimating regional and local carbon dynamics [50] and for estimating belowground carbon stocks in drylands, which are underrepresented in landscape-scale studies [51-53]. Furthermore, non-destructive root mass detection and phenology are vital to crop breeding programs [35]. In the rapidly growing field of

GPR and root detection, there exist many areas for future research. Many past root detection studies have focused investigations on large woody roots and fine root masses. High-throughput GPR studies is still a burgeoning area of research, but is needed to improve genetic selection processes in plant breeding program [54]. Ground penetrating radar has the capacity to collect in-situ root mass data iteratively, if done with high spatial accuracy, and has the potential to detect variations in root structure and growth over time, as electromagnetic radiation interaction varies between healthy roots and stressed roots. Future research in crop breeding studies may strive to detect genotype variation in root phenology by testing various frequencies.

In research to date, GPR has only been used for detection of salinity concentration but has not been investigated thoroughly [55,56]. A future study might investigate GPR sensitivity by testing multiple frequencies with a variety of soil characteristics that are useful for crop breeders or are significant to agricultural production. How GPR signal functions in the presence of different levels of salinity and sodicity, and how the signal response relates to detection of other soil characteristics in field conditions, is not yet fully understood. Furthermore, there have been no GPR-based salinity composition studies that also considered soil water content [57]. The relationship of soil composition, salinity and sodicity, and soil water content to GPR detection are areas for future research and would be of great significance for molecular breeding to develop salt-tolerant cultivars. Moreover, real-time detection of soil composition would also assist in improved resource allocation, a key component of precision agriculture.

2.6. Conclusions

This study found that above- and belowground phenology was affected differently by a gradient of salinity in the treatment plot. For genotypes PI-533752, PI-533912, and Richardson, belowground biomass production decreased relative to aboveground biomass production, contrary to my hypothesis. Additionally, this study found that the salinity was not the driving soil variable for plant height, in fact pH, B, HCO₃, and CO₃ were more influential and varied by genotype. In general, above- and belowground biomass production was greater in the medium salinity treatment for all genotypes that grew in the treatment plot that may suggest other physiological adaptations to salt-stress, or a threshold response. Overall, the Richardson Seed's Ultra-Early Hybrid and S&W Seed Sordan 79 had the widest range of growth across the salinity gradient and highest biomass and panicle production. In this study I was not able to detect root mass in highly saline-sodic soil, though, root phenology was detected with the 400MHz and 900MHz frequencies in the control plot. The GPR signal return was not linear in response to a salinity gradient, but a pattern did emerge across the different salinity ranges.

Each remote sensing study has unique environmental, technological, and logistical variables that require special means for data collection, processing, and analysis. Novel applications of these technologies require innovative techniques to mitigate for variables that are not always apparent at the beginning of a study. It is through the discovery of these idiosyncrasies that new and promising studies are developed.

Acknowledgments: I would like to acknowledge the following people, Scott Huber with the Nevada Agricultural Experiment Station in Fallon, Nevada for his help facilitating and collaborating with this research; Joey Domer, Rangeland Ecologist at the University of Nevada, Reno for his technical support and assistance in the field; Casey White, graduate researcher in the Environmental Tomography & Emerging Technologies Lab at the University of Nevada, Reno for her assistance in the field and GIS support; and

Weylin Gilbert, graduate researcher in the Environmental Tomography & Emerging Technologies Lab at the University of Nevada, Reno for his assistance with data processing and editing. Thank you all for your contributions to this research.

Conflicts of Interest: The authors declare no conflict of interest.

Abbreviations

The following abbreviations are used in this manuscript:

NAES - Nevada Agricultural Experiment Station

USDA-PMC - United States Department of Agriculture Plant Materials Center

RTK - Real-time kinematic

GPR - Ground penetrating radar

TLS - Terrestrial laser scanner

FAO - Food and Agriculture Organization

SAR - Sodium adsorption ratio

ESP - Exchangeable sodium percentage

ECe - Electrical conductivity

LiDAR - Light detection-and-ranging

USDA-GBPMC - United States Department of Agriculture Great Basin Plant Materials Center

FRC - Fallon Research Center

UNR - University of Nevada, Reno's

NRCS - Natural Resources Conservation Service

FARO - FARO Focus3D X 330

IDS GeoRadar - IDS GeoRadar RIS MF Hi-Mod Dual-channel

GPS - Global positioning system

HH - Horizontal-horizontal

GLM - Generalized linear models

AIC - Akaike Information Criterion

References

1. Corvalán, Hales, S., McMichael, A. J., Corvalán, C., McMichael, A. J., Corvalán, C. (Carlos), & McMichael, A. J. (Anthony J. . (2005). *Ecosystems and human well-being : health synthesis*. World Health Organization.
2. United Nations: Deserts, desertification, drylands, biodiversity, climate change, the environment. Available Online at: https://www.un.org/en/events/desertification_decade/whynow.shtml (accessed on 11 August 2021).
3. Qadir, M., & Oster, J. D. (2004). Crop and irrigation management strategies for saline-sodic soils and waters aimed at environmentally sustainable agriculture. *Elsevier B.V.*
4. Zomer, Trabucco, A., Bossio, D. A., & Verchot, L. V. (2008). Climate change mitigation: A spatial analysis of global land suitability for clean development mechanism afforestation and reforestation. *Agriculture, Ecosystems & Environment*, 126(1), 67–80.
<https://doi.org/10.1016/j.agee.2008.01.014>
5. Cao, Li, Y., Liu, B., Kong, F., & Tran, L.-S. P. (2018). Adaptive Mechanisms of Soybean Grown on Salt-Affected Soils: Salt Adaptation in Soybean. *Land Degradation & Development*, 29(4), 1054–1064.
<https://doi.org/10.1002/ldr.2754>
6. Costanza, de Groot, R., Sutton, P., van der Ploeg, S., Anderson, S. J., Kubiszewski, I., Farber, S., & Turner, R. K. (2014). Changes in the global value of ecosystem services. *Global Environmental Change*, 26, 152–158. <https://doi.org/10.1016/j.gloenvcha.2014.04.002>
7. Huang, Yu, H., Guan, X., Wang, G., & Guo, R. (2016). Accelerated dryland expansion under climate change. *Nature Climate Change*, 6(2), 166–171. <https://doi.org/10.1038/nclimate2837>
8. Maestre, Eldridge, D. J., Soliveres, S., Kéfi, S., Delgado-Baquerizo, M., Bowker, M. A., García-Palacios, P., Gaitán, J., Gallardo, A., Lázaro, R., & Berdugo, M. (2016). Structure and Functioning of Dryland Ecosystems in a Changing World. *Annual Review of Ecology, Evolution, and Systematics*, 47(1), 215–237. <https://doi.org/10.1146/annurev-ecolsys-121415-032311>

9. Berdugo, Delgado-Baquerizo, M., Soliveres, S., Hernández-Clemente, R., Zhao, Y., Gaitán, J. J., Gross, N., Saiz, H., Maire, V., Lehmann, A., Rillig, M. C., Solé, R. V., & Maestre, F. T. (2020). Global ecosystem thresholds driven by aridity. *Science (American Association for the Advancement of Science)*, 367(6479), 787–790. <https://doi.org/10.1126/science.aay5958>
10. Galieni, A., D'Ascenzo, N., Stagnari, F., Pagnani, G., Xie, Q., & Pisante, M. (2020;2021). Past and future of plant stress detection: An overview from remote sensing to positron emission tomography. *Frontiers in Plant Science*, 11, 609155-609155.
11. Jat, H. S., Datta, A., Sharma, P. C., Kumar, V., Yadav, A. K., Choudhary, M., Choudhary, V., Gathala, M. K., Sharma, D. K., Jat, M. L., Yaduvanshi, N. P. S., Singh, G., & McDonald, A. (2018). Assessing soil properties and nutrient availability under conservation agriculture practices in a reclaimed sodic soil in cereal-based systems of North-West India. *Archiv Für Acker- Und Pflanzenbau Und Bodenkunde*, 64(4), 531-545.
12. O'Brien, D. (2016). Tapping sorghum's genetic potential. *Agricultural Research*, 64(9), 1-2. Retrieved from <https://unr.idm.oclc.org/login?url=https://www-proquest-com.unr.idm.oclc.org/scholarly-journals/tapping-sorghums-genetic-potential/docview/1819944293/se-2?accountid=452>
13. United Sorghum Checkoff Program: All About Sorghum, 2016. Available Online: <https://www.sorghumcheckoff.com/all-about-sorghum> (accessed on 21 May 2021).
14. Bharti, A. K., Rokhsar, D. S., Schmutz, J., Grimwood, J., Kresovich, S., Peterson, D. G., Maher, C. A., Paterson, A. H., Lyons, E., Otiillar, R. P., Grigoriev, I. V., Feltus, F. A., Dubchak, I., Ming, R., Tang, H., Hellsten, U., Mehboob-ur-Rahman, Bowers, J. E., Narechania, A., ... Keller, B. (2009). The Sorghum bicolor genome and the diversification of grasses. *Nature (London)*, 457(7229), 551–556. <https://doi.org/10.1038/nature07723>
15. McGinnis, M. J., & Painter, J. E. (2020). Sorghum: History, Use, and Health Benefits. *Nutrition Today (Annapolis)*, 55(1), 38–44. <https://doi.org/10.1097/NT.0000000000000391>
16. Morris, G. P., Ramu, P., Deshpande, S. P., Hash, C. T., Shah, T., Upadhyaya, H. D., Riera-Lizarazu, O., Brown, P. J., Acharya, C. B., Mitchell, S. E., Harriman, J., Glaubitz, J. C., Buckler, E. S., &

- Kresovich, S. (2013). Population genomic and genome-wide association studies of agroclimatic traits in sorghum. *Proceedings of the National Academy of Sciences - PNAS*, 110(2), 453–458.
<https://doi.org/10.1073/pnas.1215985110>
17. Fang, Y., & Xiong, L. (2015). General mechanisms of drought response and their application in drought resistance improvement in plants. *Cellular and Molecular Life Sciences : CMLS*, 72(4), 673–689. <https://doi.org/10.1007/s00018-014-1767-0>
 18. Schaetzl, R. J. and Thompson, M. L. (2016). *Soils: Genesis and geomorphology* (Second edition). Cambridge University Press.
 19. Cuevas, Daliakopoulos, I. N., Fernando del Moral, Hueso, J. J., & Tsanis, I. K. (2019). A Review of Soil-Improving Cropping Systems for Soil Salinization. *Agronomy (Basel)*, 9(6), 295–. <https://doi.org/10.3390/agronomy9060295>
 20. Amini, Ghadiri, H., Chen, C., & Marschner, P. (2016). Salt-affected soils, reclamation, carbon dynamics, and biochar: a review. *Journal of Soils and Sediments*, 16(3), 939–953. <https://doi.org/10.1007/s11368-015-1293-1>
 21. Öztürk, Waisel, Y., Khan, M. A., & Görk, G. (2006). *Biosaline Agriculture and Salinity Tolerance in Plants* (Öztürk, Y. Waisel, M. A. Khan, & G. Görk, Eds.; 1st ed. 2006.). Birkhäuser Basel. <https://doi.org/10.1007/3-7643-7610-4>
 22. Seelig, B.D. 2000. Salinity and sodicity in North Dakota soils. Extension Bulletin 57. North Dakota State University Extension Service, Fargo, ND.
 23. Ogle, D. and L. St. John. 2010. Plants for saline and sodic soil conditions. Technical Note, TN Plant Materials No. 9A. U.S. Department of Agriculture, Natural Resources Conservation Service, Boise, ID – Salt Lake City, UT. 10pp.
 24. Akpo, Ojiewo, C. O., Kapran, I., Omoigui, L. O., Diama, A., & Varshney, R. K. (2021). *Enhancing Smallholder Farmers' Access to Seed of Improved Legume Varieties Through Multi-Stakeholder Platforms: Learning from the TLIII Project Experiences in Sub-Saharan Africa and South Asia*. Springer Singapore Pte. Limited.

25. Kassam. (2003). Farming Systems and Poverty 2001: Improving Farmers' Livelihoods in a Changing World. By J. Dixon, A. Gulliver and D. Gibbon. Rome and Washington DC: FAO and the World Bank (2002), pp. 412, £27.00, ISBN 92-5-104627-1 [Review of *Farming Systems and Poverty 2001: Improving Farmers' Livelihoods in a Changing World*. By J. Dixon, A. Gulliver and D. Gibbon. Rome and Washington DC: FAO and the World Bank (2002), pp. 412, £27.00, ISBN 92-5-104627-1]. *Experimental Agriculture*, 39(1), 109–110. Cambridge University Press.
<https://doi.org/10.1017/S0014479702211059>
26. Pitman, M.G., Läuchli, A. (2002). Global Impact of Salinity and Agricultural Ecosystems. In: Läuchli, A., Lüttge, U. (eds) *Salinity: Environment - Plants - Molecules*. Springer, Dordrecht.
https://doi.org/10.1007/0-306-48155-3_1
27. Qadir, Noble, A. D., Oster, J. D., Schubert, S., & Ghafoor, A. (2005). Driving forces for sodium removal during phytoremediation of calcareous sodic and saline-sodic soils; a review. *Soil Use and Management*, 21(2), 173–180. <https://doi.org/10.1079/SUM2005312>
28. Tuyen, Lal, S. K., & Xu, D. H. (2010). Identification of a major QTL allele from wild soybean (*Glycine soja* Sieb. & Zucc.) for increasing alkaline salt tolerance in soybean. *Theoretical and Applied Genetics*, 121(2), 229–236. <https://doi.org/10.1007/s00122-010-1304-y>
29. Li, L., Zhang, Q., & Huang, D. (2014). A review of imaging techniques for plant phenotyping. *Sensors (Basel, Switzerland)*, 14(11), 20078–20111.
30. LEFSKY, COHEN, W. B., PARKER, G. G., & HARDING, D. J. (2002). Lidar Remote Sensing for Ecosystem Studies: Lidar, an emerging remote sensing technology that directly measures the three-dimensional distribution of plant canopies, can accurately estimate vegetation structural attributes and should be of particular interest to forest, landscape, and global ecologists. *Bioscience*, 52(1), 19–30. [https://doi.org/10.1641/0006-3568\(2002\)052\[0019:LRSFES\]2.0.CO;2](https://doi.org/10.1641/0006-3568(2002)052[0019:LRSFES]2.0.CO;2)
31. Tilly, N., Hoffmeister, D., Schiedung, H., Hütt, C., Brands, J., & Bareth, G. (2014). Terrestrial laser scanning for plant height measurement and biomass estimation of maize. *International Archives of the Photogrammetry, Remote Sensing and Spatial Information Sciences.*, XL(7), 181–187.

32. Friedli, M., Kirchgessner, N., Grieder, C., Liebisch, F., Mannale, M., & Walter, A. (2016). Terrestrial 3D laser scanning to track the increase in canopy height of both monocot and dicot crop species under field conditions. *Plant Methods*, *12*(1), 9-9.
33. Fang, Y., Qiu, X., Guo, T., Wang, Y., Cheng, T., Zhu, Y., Chen, Q., Cao, W., Yao, X., Niu, Q., Hu, Y., & Gui, L. (2020). An automatic method for counting wheat tiller number in the field with terrestrial LiDAR. *Plant Methods*, *16*(1), 1-132.
34. Liu, X., Dong, X., Xue, Q., Leskovar, D. I., Jifon, J., Butnor, J. R., & Marek, T. (2018). Ground penetrating radar (GPR) detects fine roots of agricultural crops in the field. *Plant and Soil*, *423*(1), 517-531.
35. Delgado, Hays, D. B., Bruton, R. K., Ceballos, H., Novo, A., Boi, E., & Selvaraj, M. G. (2017). Ground penetrating radar: a case study for estimating root bulking rate in cassava (*Manihot esculenta* Crantz). *Plant Methods*, *13*(1), 65–65. <https://doi.org/10.1186/s13007-017-0216-0>
36. Liu, X., Dong, X., & Leskovar, D. I. (2016). Ground penetrating radar for underground sensing in agriculture: A review. *International Agrophysics*, *30*(4), 533-543.
37. Doolittle, James A.; Butnor, John R. 2009. Soils, peatlands, and biomonitoring. In: Ground Penetrating Radar: Theory and Applications, ed. Jol, Harry; Elsevier. pp 179-202. Chapter 6.
38. Butnor, Doolittle, J. A., Kress, L., Cohen, S., & Johnsen, K. H. (2001). Use of ground-penetrating radar to study tree roots in the southeastern United States. *Tree Physiology*, *21*(17), 1269–1278.
39. USDA Natural Resources Conservation Service: Web Soil Survey. Available at: <https://websoilsurvey.nrcs.usda.gov/app/> (accessed on 15 November 2020).
40. Calone, Sanoubar, R., Lambertini, C., Speranza, M., Antisari, L. V., Vianello, G., & Barbanti, L. (2020). Salt Tolerance and Na Allocation in Sorghum bicolor under Variable Soil and Water Salinity. *Plants (Basel)*, *9*(5), 561–. <https://doi.org/10.3390/plants9050561>
41. FARO Technologies. (2021). FARO Scene. Available at: <https://www.faro.com/products/faro-software/faro-scene/>

42. CloudCompare (version: 2.11.1 Anoa) [GNU GPL software Windows 64-bit]. Retrieved from: <http://www.cloudcompare.org/>
43. QGIS Development Team, (2022). QGIS Geographic Information System (version 3.32.1). Open Source Geospatial Foundation Project. Retrieved from: <http://qgis.osgeo.org>
44. RStudio Team. (1 July 2022). RStudio: Integrated Development Environment for R. RStudio, PBC (version 3) [GNU Affero GPL]. Retrieved from: <https://www.rstudio.com/>
45. Topp, Davis, J. L., & Annan, A. P. (1980). Electromagnetic determination of soil water content; measurements in coaxial transmission lines. *Water Resources Research*, 16(3), 574–582.
46. Machwitz, Pieruschka, R., Berger, K., Schlerf, M., Aasen, H., Fahrner, S., Jiménez-Berni, J., Baret, F., & Rascher, U. (2021). Bridging the Gap Between Remote Sensing and Plant Phenotyping – Challenges and Opportunities for the Next Generation of Sustainable Agriculture. *Frontiers in Plant Science*, 12, 749374–749374. <https://doi.org/10.3389/fpls.2021.749374>
47. Eitel, J.U.H., Vierling, L.A., Brown, T.T., Huggins, D.R. 2014. LIDAR based biomass and crop nitrogen estimates for rapid, non-destructive assessment of wheat nitrogen status. *Field Crops Research* 159: 21-32.
48. Cobb, DeClerck, G., Greenberg, A., Clark, R., & McCouch, S. (2013). Next-generation phenotyping: requirements and strategies for enhancing our understanding of genotype–phenotype relationships and its relevance to crop improvement. *Theoretical and Applied Genetics*, 126(4), 867–887. <https://doi.org/10.1007/s00122-013-2066-0>
49. Schneider, Kükenbrink, D., Schaepman, M. E., Schimel, D. S., & Morsdorf, F. (2019). Quantifying 3D structure and occlusion in dense tropical and temperate forests using close-range LiDAR. *Agricultural and Forest Meteorology*, 268, 249–257. <https://doi.org/10.1016/j.agrformet.2019.01.033>
50. Zechmeister-Boltenstern, Keiblinger, K. M., Mooshammer, M., Peñuelas, J., Richter, A., Sardans, J., & Wanek, W. (2015). The application of ecological stoichiometry to plant-microbial-soil organic matter transformations. *Ecological Monographs*, 85(2), 133–155. <https://doi.org/10.1890/14-0777.1>

51. Lal, Rattan. (2004). Carbon sequestration in dryland ecosystems. *Environmental Management (New York)*, 33(4), 528–544. <https://doi.org/10.1007/s00267-003-9110-9>
52. ASNER, ARCHER, S., HUGHES, R. F., ANSLEY, R. J., & WESSMAN, C. A. (2003). Net changes in regional woody vegetation cover and carbon storage in Texas Drylands, 1937-1999. *Global Change Biology*, 9(3), 316–335. <https://doi.org/10.1046/j.1365-2486.2003.00594.x>
53. Washington-Allen, West, N. E., Ramsey, R. D., & Efrogmson, R. A. (2006). A Protocol for Retrospective Remote Sensing–Based Ecological Monitoring of Rangelands. *Rangeland Ecology & Management*, 59(1), 19–29. <https://doi.org/10.2111/04-116R2.1>
54. Jangra, Chaudhary, V., Yadav, R. C., & Yadav, N. R. (2021). High-Throughput Phenotyping: A Platform to Accelerate Crop Improvement. *Phenomics (Cham, Switzerland)*, 1(2), 31–53. <https://doi.org/10.1007/s43657-020-00007-6>
55. Wu, Li, X., Zhao, K., Jiang, T., Zheng, X., Li, X., Gu, L., & Wang, X. (2020). A Nondestructive Conductivity Estimating Method for Saline-Alkali Land Based on Ground Penetrating Radar. *IEEE Transactions on Geoscience and Remote Sensing*, 58(4), 2605–2614. <https://doi.org/10.1109/TGRS.2019.2952719>
56. Hagrey, A., Müller, & Christian-Albrechts-Univ., K. (2000). GPR study of pore water content and salinity in sand. *Geophysical Prospecting*, 48(1), 63-85.
57. Huisman, Hubbard, S. S., Redman, J. D., & Annan, A. P. (2003). Measuring soil water content with ground penetrating radar; a review. *Vadose Zone Journal*, 2(4), 476–491. <https://doi.org/10.2113/2.4.476>